Ground structure imaging by inversions of Rayleigh wave ellipticity: sensitivity analysis and application to European strong-motion sites

M. Hobiger, C. Cornou, M. Wathelet, G. Di Giulio, B. Knapmeyer-Endrun, F. Renalier, Pierre-Yves Bard, A. Savvaidis, S. Hailemikael, N. Le, et al.

Geophysical Journal International

Geophys. J. Int. (2013) **192,** 207–229 doi: 10.1093/gji/ggs005

Ground structure imaging by inversions of Rayleigh wave ellipticity: sensitivity analysis and application to European strong-motion sites

M. Hobiger,[1,*] C. Cornou,[1] M. Wathelet,[1] G. Di Giulio,[2,3] B. Knapmeyer-Endrun,[4] F. Renalier,[1] P.-Y. Bard,[1] A. Savvaidis,[2] S. Hailemikael,[5] N. Le Bihan,[6] M. Ohrnberger[4] and N. Theodoulidis[2]

[1]*Institut des Sciences de la Terre (ISTerre), IRD, IFSTTAR, CNRS, Université de Grenoble I, France. E-mail: manuel.hobiger@bgr.de*
[2]*Institute of Engineering Seismology and Earthquake Engineering (ITSAK - EPPO), Thessaloniki, Greece*
[3]*Istituto Nazionale di Geofisica e Vulcanologia (INGV), Rome, Italy*
[4]*Institut für Geowissenschaften, Universität Potsdam, Germany*
[5]*Dipartimento della Protezione Civile, Rome, Italy*
[6]*GIPSA-Lab, CNRS, Grenoble, France*

Accepted 2012 October 4. Received 2012 October 3; in original form 2012 January 6

SUMMARY

The knowledge of the local soil structure is important for the assessment of seismic hazards. A widespread, but time-consuming technique to retrieve the parameters of the local underground is the drilling of boreholes. Another way to obtain the shear wave velocity profile at a given location is the inversion of surface wave dispersion curves. To ensure a good resolution for both superficial and deeper layers, the used dispersion curves need to cover a wide frequency range. This wide frequency range can be obtained using several arrays of seismic sensors or a single array comprising a large number of sensors. Consequently, these measurements are time-consuming. A simpler alternative is provided by the use of the ellipticity of Rayleigh waves. The frequency dependence of the ellipticity is tightly linked to the shear wave velocity profile. Furthermore, it can be measured using a single seismic sensor. As soil structures obtained by scaling of a given model exhibit the same ellipticity curve, any inversion of the ellipticity curve alone will be ambiguous. Therefore, additional measurements which fix the absolute value of the shear wave velocity profile at some points have to be included in the inversion process. Small-scale spatial autocorrelation measurements or MASW measurements can provide the needed data. Using a theoretical soil structure, we show which parts of the ellipticity curve have to be included in the inversion process to get a reliable result and which parts can be omitted. Furthermore, the use of autocorrelation or high-frequency dispersion curves will be highlighted. The resulting guidelines for inversions including ellipticity data are then applied to real data measurements collected at 14 different sites during the European NERIES project. It is found that the results are in good agreement with dispersion curve measurements. Furthermore, the method can help in identifying the mode of Rayleigh waves in dispersion curve measurements.

Key words: Inverse theory; Surface waves and free oscillations; Site effects; Computational seismology; Wave propagation.

1 INTRODUCTION

To assess the seismic hazard of a given site, it is important to know the shear wave velocity structure down to a certain depth. In most seismic codes, the average velocity to reach a depth of 30 m (Vs30) is used for site classification. For the evaluation of the site response, the velocity profile down to the seismic bedrock has to be known. The local soil structure can be investigated by different means. The drilling of boreholes gives a good view of the underground structure, but is a time-consuming task, especially for investigations over large areas. Refraction or reflection measurements using vibration sources can also be carried out in urban areas, but still need much effort. On the contrary, active sources like sledgehammering generate waves only in a high frequency range which does not penetrate the soil very deeply. Although it is suitable for estimating Vs30 or the

*Now at: Bundesanstalt für Geowissenschaften und Rohstoffe (BGR), Stilleweg 2, 30655 Hannover, Germany.

shear wave velocity profile for shallow bedrock sites, this technique does not allow retrieving the shear wave velocity structure down to the seismic bedrock for sediments of several tens or hundreds of metres thickness. In such a case, the use of seismic ambient vibrations is an appropriate alternative. Arrays of seismic sensors can indeed be easily deployed to measure dispersion curves of surface waves which can be inverted for the local soil structure. However, several seismic arrays have to be deployed to cover a wavelength range wide enough to retrieve the shear wave structure down to the seismic bedrock (Wathelet *et al.* 2008). As a result, such measurements are time-consuming. In urban areas, the existing infrastructure also limits the possible deployment locations of seismic sensors. Therefore, the development of methods which limit the actual number of sensors to a minimum is appealing.

The ellipticity of Rayleigh waves, that is, the ratio between the horizontal and the vertical particle motions, strongly depends on the local soil structure and carries information on the complete sedimentary layers. Although ellipticity measurements have already been used by Boore & Toksöz (1969) to infer the ground structure, it is only during the last few years that this topic has regained larger interest for both shallow (Yamanaka *et al.* 1994; Fäh *et al.* 2001; Satoh *et al.* 2001; Scherbaum *et al.* 2003; Malischewsky & Scherbaum 2004; Tuan *et al.* 2011) and lithospheric structure imaging (Tanimoto & Alvizuri 2006; Ferreira & Woodhouse 2007; Yano *et al.* 2009). A widespread technique for investigating the soil structure is the classical H/V technique (Nogoshi & Igarashi 1971; Nakamura 1989). The H/V ratio simply indicates the spectral ratio between the horizontal and the vertical components. Sánchez-Sesma *et al.* (2011) established a link between the H/V ratio and the sensor component's autocorrelation Green's functions for perfectly equipartitioned wavefields. If the wavefield was composed exclusively of single mode Rayleigh waves, the H/V ratio and ellipticity should be the same. In general, however, the seismic noise wavefield is composed of different modes of Rayleigh and Love waves and of body waves. It has been numerically shown that the composition of the noise wavefield actually depends on the noise sources and the site structure (Bonnefoy-Claudet *et al.* 2008; Albarello & Lunedei 2010). Seismic noise recordings have shown that the relative contribution of Love and Rayleigh waves to the noise wavefield varies from site to site (Köhler *et al.* 2006; Endrun 2011). As a consequence, the H/V ratio provides, in general, an overestimation of the actual ellipticity of Rayleigh waves (Poggi *et al.* 2012).

Assuming the wavefield composition, the H/V curve can be corrected for Love wave contributions and the resulting curve can be interpreted and inverted as an ellipticity curve (Fäh *et al.* 2001, 2003; Poggi *et al.* 2012). Scherbaum *et al.* (2003) showed that the inversion of Rayleigh wave dispersion curves can be improved by including the H/V peak and trough frequencies in the inversion process. Arai & Tokimatsu (2004) showed the possibility of inverting H/V curves to retrieve the layer thicknesses of the shear wave velocity profile in case that the absolute velocities are known and vice versa. Parolai *et al.* (2005) inverted Rayleigh wave dispersion curves jointly with H/V curves, assuming equal absolute loading forces on the vertical and horizontal components. A similar study was performed by Picozzi *et al.* (2005), who concluded that an inversion of the dispersion curve constrains the sedimentary velocity profile, whereas an inclusion of the H/V curve sets additional constraints on bedrock depth and velocity due to the correlation between the H/V amplitude and the impedance contrast. Arai & Tokimatsu (2005) also showed the benefits of including the H/V curve in the inversion of Rayleigh wave dispersion curves. Furthermore, they proposed to use H/V data and small-scale array measurements instead of large-scale array measurements which are necessary to obtain broad-band dispersion curves.

However, inversions of H/V curves always require prior assumptions on the energy partition between Love and Rayleigh waves in the noise wavefield, or on the ratio of horizontal and vertical loading forces. Recent studies have shown that the energy partition is, even for a given site, not constant and varies with frequency and time (Köhler *et al.* 2006; Endrun 2011). By directly extracting the ellipticity from the noise wavefield, any assumptions on the Love and Rayleigh wave contributions on the wavefield composition could be avoided in the subsequent inversion.

Newly developed techniques allow the direct retrieval of Rayleigh wave ellipticity from noise recordings. The RayDec method (Hobiger *et al.* 2009) uses the random decrement technique (Asmussen 1997) which is usually applied to measure the resonance frequencies and damping parameters of buildings (Dunand 2005; Michel *et al.* 2008). This technique stacks large numbers of vertical and horizontal signals and correlates them in a particular way to enhance Rayleigh waves and suppress Love and body wave contributions.

Poggi & Fäh (2010) extracted fundamental and higher modes of ellipticity by applying a three-component version of the high-resolution frequency-wavenumber method (Capon 1969) to seismic array recordings. Recently, Poggi *et al.* (2012) applied a continuous wavelet transform approach to the noise wavefield recorded at a single site to extract the Rayleigh waves. Another new technique was proposed by Maranò *et al.* 2012 who developed a maximum likelihood three-component array method for extracting Rayleigh and Love wave dispersion curves together with the ellipticity of Rayleigh waves.

Nevertheless, ellipticity measurements alone are never sufficient to retrieve the local soil structure. By scaling both the wave velocity and the depth values of a given soil structure model by the same factor, the ellipticity function remains the same (Scherbaum *et al.* 2003). Fig. 1 shows that different shear wave velocity structures can provide the same ellipticity curve. These velocity models were obtained by scaling the depth, shear and pressure wave velocities by the same factor. It is thus obvious that an ellipticity inversion alone would yield ambiguous results by fixing the shape of the velocity profile only, but not the absolute scale. If information constraining the superficial shear wave structure is added, the ellipticity inversion can then be used to constrain the deeper part of the structure. Fixing the shear wave velocities at the surface can be easily done by using small-scale passive [SPAC: spatial autocorrelation, Aki (1957); frequency-wavenumber technique, Capon (1969)] or active measurements such as MASW (Multichannel analysis of surface waves, Park *et al.* 1999; Socco & Strobbia 2004).

Although the inversion of ellipticity may definitely help in imaging the ground structure, so far no study has been performed to investigate which part of the ellipticity curve is actually carrying the most relevant information to be inverted, how biases in the ellipticity estimation affect the resulting shear wave profiles and how the ellipticity data should be combined with additional information on the superficial shear wave structure. In this paper, we want to explore the possibilities and limits of the approach already suggested by Arai & Tokimatsu (2005), that is, to fix the superficial shear wave structure using data such as small-scale SPAC measurements or high-frequency MASW dispersion curves and use the ellipticity information to further constrain the deeper structure. The measurements necessary for this approach would be far easier and faster to perform than in the common approach of measuring broad-band

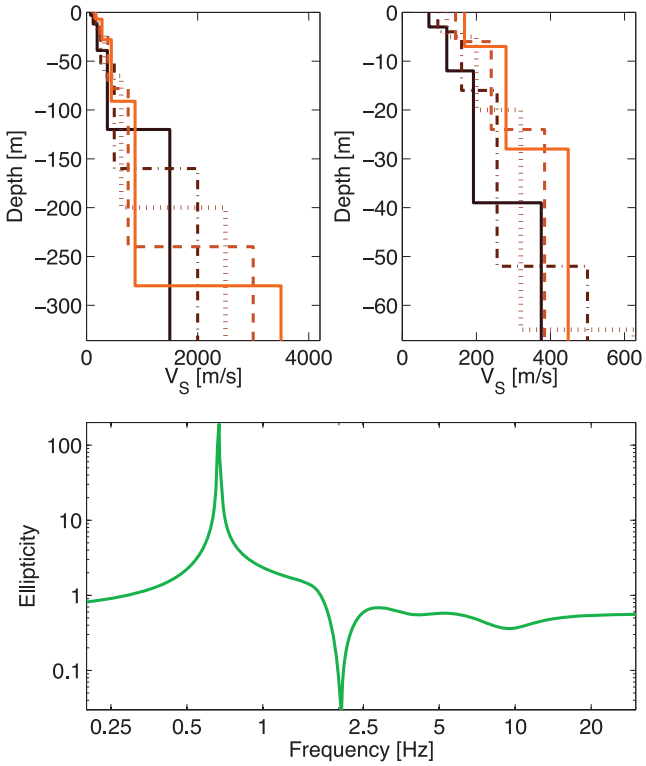

Figure 1. (Top left-hand side) Five different soil models which can be transformed one into another by multiplying the depth, shear and pressure waves by the same factor. (Top right-hand side) Zoom on the upper layers. (Bottom) The five models have the same corresponding ellipticity curve.

dispersion curves by deploying multiple seismic arrays of different size.

The first part of this paper will focus on the theoretical aspects of joint inversion of the Rayleigh wave ellipticity and near-surface dispersion data for ground models with and without singularities in the ellipticity curve. Multiple ellipticity peaks can result from multiple strong impedance contrasts in the ground structure or of higher mode dominance in certain frequency ranges as possible signature of low-velocity zones. However, several numerical and experimental studies at well-known sites have shown that the energy of the Rayleigh-wave fundamental mode strongly dominates in the frequency range corresponding to the right flank of the H/V spectral ratio (e.g. Konno & Ohmachi 1998; Bonnefoy-Claudet *et al.* 2008; Albarello & Lunedei 2011; Uebayashi *et al.* 2012). The theoretical section will thus focus on the ellipticity of the fundamental mode only with the aim to investigate which parts of the soil structure can be recovered by such joint inversions, which parts of the ellipticity actually carry the most valuable information for the inversion and whether inverting the right flank of ellipticity leads to an accurate estimation of the shear wave velocity profile. We will thus neglect the possibility of higher mode dominance in certain frequency ranges and the possibility of low-velocity zones for the sake of simplicity. We refer the interested reader to papers on dispersion curve inversion in cases of higher mode domination in certain frequency ranges (Cercato 2009, 2011) and papers on the influence of low-velocity zones on dispersion curve inversions (Calderón-Macías & Luke 2007; Liang *et al.* 2008; Cercato *et al.* 2010).

The inferred rules for ellipticity inversions will then be applied to ambient noise recordings at 14 European sites for which broad-band dispersion curves, autocorrelation curves and borehole data are available. In that section, our objective will be to compare dispersion curves inferred from the joint inversion of autocorrelation and ellipticity curves with the broad-band measured dispersion curves. The proximity to the actual dispersion curves will be the measure of the integrity of the inversions.

2 TESTS ON THEORETICAL DATA

2.1 Ground models, inversion algorithm and integrity of fit

To investigate which parts of the ellipticity curve have to be included or may be omitted in the inversion and how biased ellipticity estimates influence the inversion results, we performed inversion tests on theoretical data obtained for two extreme and rather simple ground structures which provide theoretical ellipticity curves with and without singularities (peaks and troughs). The presence of peaks and troughs in the ellipticity curve is mainly controlled by the *S*-wave impedance contrast between the sedimentary layers and the underlying seismic bedrock. For high *S*-wave impedance constrasts, the ellipticity exhibits peaks and troughs, corresponding to a reversal of the sense of rotation, while for low contrasts, no such singularities occur (e.g. Malischewsky & Scherbaum (2004); Tuan *et al.* (2011)). For the model with ellipticity singularities (model A, see Figs 2a and b), we used a simplified version of the soil structure model of the Euroseistest site in Volvi, Greece (Raptakis *et al.* 1998). We fixed the number of layers to four overlying a homogeneous half-space. By changing the shear and pressure wave velocities of the fourth and fifth layers of model A, and consequently reducing the impedance contrast, we obtained model B (Figs 2c and d) which does not exhibit ellipticity singularities. Consequently, models A and B only differ for depths larger than 60 m. Table 1 summarizes the parameters of both soil profiles.

As mentioned in the introduction, due to the non-uniqueness of the ellipticity information, any ellipticity inversion needs further constraints, for example, parts of the shear wave profile or surface wave data for the near-surface. In the following, we use theoretical SPAC curves calculated using models A and B for circular arrays of 5 and 10 m radius, respectively, in the frequency range between 2 and 30 Hz. For arrays of such small sizes, the SPAC curves of models A and B are identical in this frequency range.

The exact theoretical dispersion and SPAC curves are calculated using a fast formulation of Dunkin (1965), following the eigenvalue problem described in Thomson (1950) and Haskell (1953). Ellipticity is computed from the full stack of the eigenvalues and the fast root search algorithm is stopped when the dispersion curve is estimated with a relative precision of 10^{-7} (Wathelet 2005). The inversions are performed using the Conditional Neighbourhood Algorithm (Wathelet *et al.* 2004; Wathelet 2008), which is a modified version of the Neighbourhood Algorithm (Sambridge 1999a,b). For a random initial set of models, the associated misfit values are calculated. The next generation of models is located in the neighbourhood of the models with the lowest misfit values. In this way, the search is guided by the best models without neglecting the possible existence of better-fitting models further away. The associated misfit value for a model with associated values M_i is calculated by

$$\text{misfit} = \sqrt{\frac{1}{N} \cdot \sum_{i=1}^{N} \left(\frac{D_i - M_i}{\sigma_i} \right)^2}, \qquad (1)$$

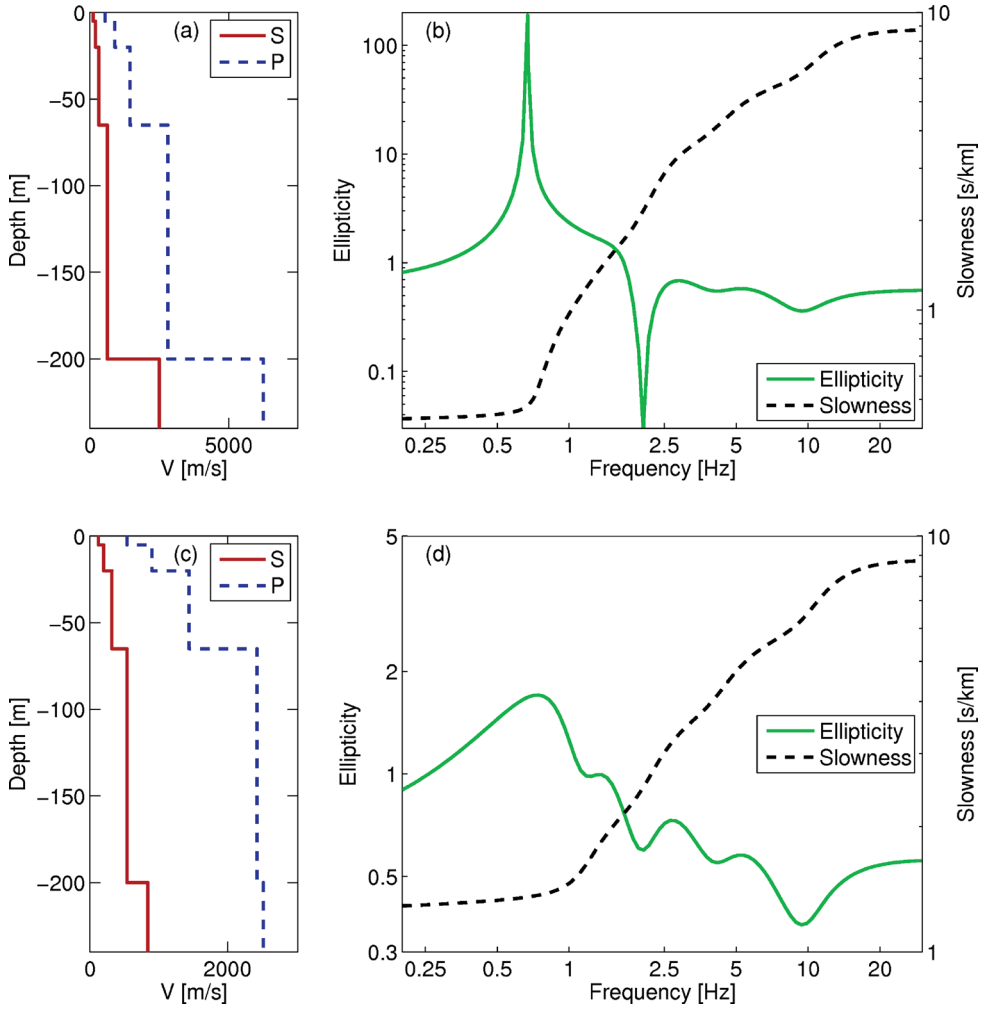

Figure 2. (a) Pressure and shear wave velocities of the sample ground structure profile of model A, (b) the corresponding dispersion and ellipticity curves. (c) Pressure and shear wave velocity profiles of model B, (d) the corresponding dispersion and ellipticity curves.

Table 1. Table of the parameters of the used soil profile models A and B.

	Thickness (m)	Depth range (m)	Model A		Model B		ρ
			V_P(m s^{-1})	V_S(m s^{-1})	V_P(m s^{-1})	V_S(m s^{-1})	(kg m^{-3})
layer 1	5	0–5	540	120	540	120	1800
layer 2	15	5–20	900	200	900	200	1800
layer 3	45	20–65	1440	320	1440	320	1800
layer 4	135	65–200	2810	625	2430	540	1800
layer 5	∞	>200	6250	2500	2520	840	2000

if the measured data to be inverted is given by a set of N data points D_i ($1 \leq i \leq N$) with associated measuring errors σ_i. For the inversions of theoretical data presented in the following, we assume equal measuring errors for each data point. An arbitrary choice of the value of σ_i only scales the misfit value and we fix it, for the sake of simplicity, to 1. If two different data sets, for example, a SPAC and an ellipticity curve, are to be inverted jointly, a separate misfit value will be calculated for each of them and the final misfit value will be a weighted average of both values. In this paper, we will impose equal weights on both information. Indeed, the aim of this paper is to investigate joint inversions of ellipticity and additional knowledge on the near-surface dispersion data to obtain reliable information on the entire ground profile. Therefore, ellipticity and additional data will, in most cases, cover different frequency ranges. Thus, there is no reason to consider different weights during the inversion. For inversions of ellipticity values, the logarithm of the ellipticity value is used instead of the absolute value.

For the inversions performed in the theoretical part of this paper, the number of layers in the inversion was always fixed to four layers over a homogeneous half-space, the correct parameterization for the used ground structure models. For simpler structure models with less parameters, the inversion should be faster, that is, converge after less generated models. This paper focuses on the possibilities and limits of ellipticity inversions and a study of the effects of different parametrizations would be far beyond its scope (Di Giulio *et al.* 2012).

The parameter space of the inversion is selected in such a way that the shear- and pressure-wave velocities and the layer thicknesses

can vary in a broad range around the actual structure model. The Poisson's ratio is confined to the range from 0.2 to 0.5 for all layers, thus limiting the ratio between pressure and shear wave velocities. The inversion's parameter range is therefore 14-dimensional for the case of four layers overlying a homogeneous half-space (five shear- and five pressure-wave velocities, four depths). Low-velocity zones are not allowed in the inversion, the shear- and pressure-wave velocities are constrained to increase with depth. The density of the different layers is fixed to $2\,000\,\mathrm{kg\,m^{-3}}$ for all layers. As the actual structure model (with a misfit value of 0) is always included in the parameter space, all of our theoretical inversions should yield this model after a sufficiently long inversion time, if the data points used in the inversion constrain the ground structure sufficiently. However, the complete exploration of the parameter space would take an infinite time, even if the used inversion algorithm converges faster than Monte-Carlo algorithms. Anyhow, the goal of a seismic inversion is to find a model with a good fit to the data within a reasonable time. Therefore, all of the inversions in the theoretical section include the same number of generated models (100 100, as the convergence for most models is good after this time). Differences in the integrity of the fit for the different inversions can therefore be assigned to difficulties to actually fit certain data points, which slow down the inversion. For inversions of real data, such data points would also slow down the inversion speed. Therefore, the results of the following theoretical section are valuable for the inversion of real measured data.

As the inversions in this section are performed for theoretical curves, we know the exact soil structure and can therefore directly investigate how good the model is fitted. Therefore, it is desirable to define a parameter describing the integrity of fit. This parameter should be applicable without much adjustment for real data inversions as well. Computing the integrity of fit by comparing the inverted shear wave profiles with the theoretical one would be problematic. Indeed, the reference model and the inverted model may not have exactly the same layer thicknesses and bedrock depth. The choice of the depth down to which the models are compared would then strongly influence the integrity of fit.

Therefore, a better alternative is to compare the Rayleigh wave dispersion curve calculated for the inverted models with a reference dispersion curve. This reference dispersion curve can be calculated for the given theoretical model. Similarly to the definition of the misfit value, we define a proximity value comparing inverted and theoretical dispersion curves at N frequency samples by

$$T = \sqrt{\frac{1}{N}\sum_{i=1}^{N}\left(\frac{s_{\mathrm{mod}}(f_i) - s_{\mathrm{inv}}(f_i)}{s_{\mathrm{mod}}(f_i)}\right)^2}. \qquad (2)$$

Here, $s_{\mathrm{inv}}(f)$ indicates the dispersion curve for the inverted models and $s_{\mathrm{mod}}(f)$ the theoretical dispersion curve for the given structure where the dispersion curves are expressed in slowness. As the theoretical models do not have measuring errors, σ_i from eq. (1) is replaced by $s_{\mathrm{mod}}(f_i)$ in eq. (2). In this way, T gives a sort of mean deviation of the inversion model from the reference model and describes the integrity of fit. For the theoretical models, we define that values of T below 0.1 are acceptable and values below 0.05 indicate a good fit.

2.2 Parts of the ellipticity curve carrying the most valuable information

In the following inversions, the theoretical SPAC curves for radii of 5 or 10 m (between 2 and 30 Hz with valuable information above about 4 Hz) and the theoretical ellipticity curves of model A and B will be inverted jointly. To determine which parts of the ellipticity curve carry the important information on the soil structure, different parts of the ellipticity curve will be used for the inversion process and the results will be compared for both a model with and without singularities (peak and trough) in the ellipticity curve.

2.2.1 Inversion of an ellipticity curve exhibiting singularities (model A)

The theoretical ellipticity curve of model A exhibits a peak at 0.67 Hz and a trough at 2.05 Hz. Although we have performed numerous inversions involving different parts of the ellipticity curves (Hobiger 2011), we will only present the most relevant inversions here.

In general, any ellipticity estimation technique relies on a correlation analysis between the vertical and horizontal components of ambient vibrations (Tanimoto & Alvizuri 2006; Hobiger *et al.* 2009; Poggi & Fäh 2010). Such estimations are prone to misestimations at the singularities (i.e. peaks and troughs). As Love waves are only present on the horizontal components, this effect is more pronounced at the trough, where the Rayleigh wave contribution to the horizontal component vanishes. Above the trough frequency, the influence of higher modes might also lead to misestimations of the different Rayleigh mode ellipticities. As the right flank of the ellipticity is thus the most reliable part of an ellipticity measurement, we will focus on the results for inverting different parts of the right flank. For comparison reasons, an inversion of the sole autocorrelation data and an inversion including the left flank of the ellipticity peak are also shown.

Fig. 3 shows the results obtained by inverting different parts of the ellipticity curve. The misfit and T values of the best-fitting models of these inversions are given in Table 2. The T values are calculated for the frequency range between 0.7 and 30 Hz, but the curves are also shown for lower frequencies. As the best-fitting model alone is not necessarily representative for the set of best-fitting models, we also calculated the T values for all generated models with misfit values lower than 1.05 times the minimum misfit value. Additionally to the T value of the best-fitting model, the maximum T value of this population of models is then a good indicator of the inversion integrity.

Fig. 3(a) shows the results of the inversion of the autocorrelation curve only, without considering ellipticity information. Although the autocorrelation curve is well fitted and the T value is low, only the superficial layers are well constrained and fit the true model. For depths larger than 50 m, however, the shear wave is hardly constrained. When considering the corresponding Rayleigh wave dispersion curves, only the higher frequency part above 2 Hz is well constrained.

Including the left flank of the ellipticity in the inversion (Fig. 3b), the true ground structure is not retrieved. Although the low minimum misfit value indicates that the inversion targets are well fitted, the generated ellipticity curves are badly constrained above the peak frequency and the dispersion curves exhibit a large variability over the whole frequency range.

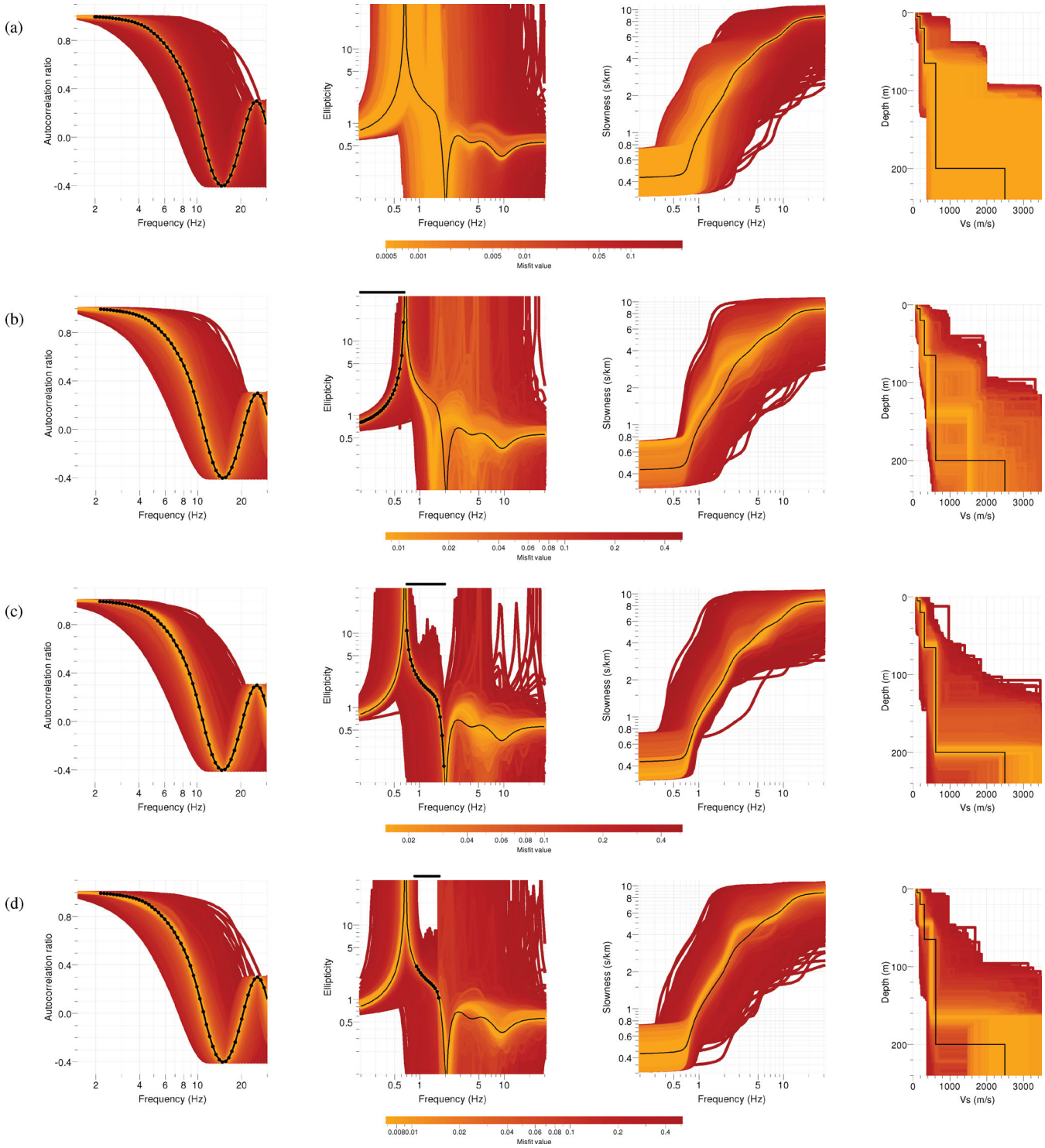

Figure 3. Inversion results for joint inversions of the SPAC curve (left-hand side) and the ellipticity curve (centre left): dispersion curves (centre right) and shear wave velocity profiles (right-hand side). The data points used for the inversion are shown as black dots, the curves corresponding to the true model as solid lines. The black bars above the ellipticity curves indicate the frequency range used for the inversion. All generated models are plotted one above each other, the best-fitting models with lowest misfits on top. The colour scale represents the misfit of the single models, lighter colours indicating lower misfit values. (a) Inversion of the SPAC data only. (b–f) Joint inversions of the SPAC and ellipticity data (b) between 0.2 and 0.65 Hz, (c) between 0.7 and 2 Hz, (d) between 0.9 and 1.7 Hz, (e) between 0.7 and 1.7 Hz and 2.5 and 4.0 Hz, (f) between 0.9 and 1.7 Hz using the autocorrelation curve for a 10-m ring.

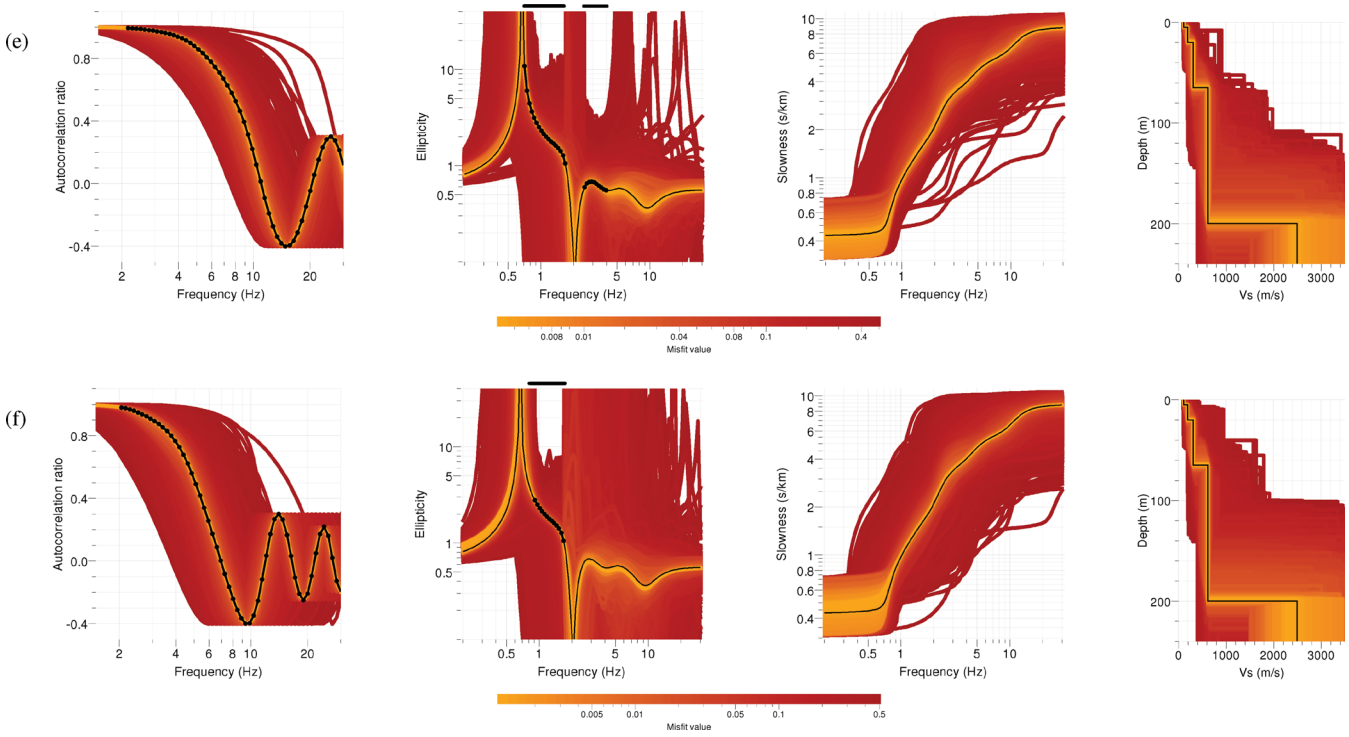

Figure 3. (*Continued.*)

Table 2. Parts of the autocorrelation and ellipticity curves used for the inversions and the associated misfit for the best-fitting models of joint inversions of autocorrelation and ellipticity curves for model A and model B. The T values for the best-fitting model and the maximum T value of all models with misfits lower than 1.05 times the minimum misfit are also indicated. 100 100 models have been generated for each inversion.

Reference figure	Autocorrelation curve		Used frequency range of the ellipticity curve	Minimum misfit	T value (0.7–30 Hz)	
	Array radius	Frequency range			best model	maximum
Fig. 3(a)	5 m	2–30 Hz	-	0.0005	0.019	0.164
Fig. 3(b)	5 m	2–30 Hz	0.2–0.65 Hz	0.0085	0.241	0.241
Fig. 3(c)	5 m	2–30 Hz	0.7–2.0 Hz	0.0154	0.043	0.043
Fig. 3(d)	5 m	2–30 Hz	0.9–1.7 Hz	0.0070	0.154	0.156
Fig. 3(e)	5 m	2–30 Hz	0.7–1.7, 2.5–4.0 Hz	0.0041	0.013	0.014
Fig. 3(f)	10 m	2–30 Hz	0.9–1.7 Hz	0.0011	0.030	0.034
Fig. 4(a)	5 m	2–30 Hz	-	0.0005	0.149	0.213
Fig. 4(b)	5 m	2–30 Hz	0.75–9.5 Hz	0.0070	0.017	0.019
Fig. 4(c)	5 m	2–30 Hz	0.75–5.2 Hz	0.0131	0.047	0.060
Fig. 4(d)	5 m	2–30 Hz	0.60–2.7 Hz	0.0178	0.233	0.242

Table 3. Table of the parameters of the different soil profiles used for the investigation of the gap between ellipticity and dispersion data.

	Model 1 (1 layer over half-space)			Model 2 (2 layers over half-space)			Model 3 (3 layers over half-space)			Model 4 (=Model A) (4 layers over half-space)		
Layer	Thickness (m)	Depth range (m)	V_S (m s^{-1})	Thickness (m)	Depth range (m)	V_S (m s^{-1})	Thickness (m)	Depth range (m)	V_S (m s^{-1})	Thickness (m)	Depth range (m)	V_S (m s^{-1})
A	200	0–200	540	80	0–80	270	32	0–32	180	5	0–5	120
B				120	80–200	870	48	32–80	320	15	5–20	200
C							120	80–200	750	45	20–65	320
D										135	65–200	625
bedrock	∞	>200	2500	∞	>200	2500	∞	>200	2500	∞	>200	2500

The inversion of the right flank of the ellipticity peak between 0.7 and 2.0 Hz (Fig. 3c) yields rather good results. Even the left flank of the ellipticity peak is well retrieved. Beyond the trough frequency, the ellipticity curve is badly constrained. The fit with the real dispersion curve is good and the shear wave velocity profile is well fitted as well.

In Fig. 3(d), the limitations of real ellipticity measurements are better taken into account, excluding ellipticity values above 3 and

Table 4. Parameters of the inversions used for the investigation of the influence of the gap between ellipticity and dispersion data. For each inversion, the ellipticity information between 0.45 and 0.61 Hz and between 0.74 and 1.00 Hz has been inverted. 100 100 models have been generated in each inversion.

Number of layers	Used frequency range of the dispersion curve	Minimum misfit	*T* value (0.7–30 Hz) best model	maximum
1	1–30 Hz	0.0093	0.0073	0.0073
1	2–30 Hz	0.0076	0.0073	0.0073
1	3–30 Hz	0.0075	0.0073	0.0073
1	4–30 Hz	0.0075	0.0073	0.0073
1	5–30 Hz	0.0075	0.0073	0.0073
1	6–30 Hz	0.0075	0.0073	0.0073
1	7–30 Hz	0.0075	0.0073	0.0073
1	8–30 Hz	0.0075	0.0073	0.0073
1	9–30 Hz	0.0075	0.0073	0.0073
1	10–30 Hz	0.0075	0.0073	0.0073
2	1–30 Hz	0.0051	0.0062	0.0062
2	2–30 Hz	0.0050	0.0062	0.0062
2	3–30 Hz	0.0052	0.0062	0.0062
2	4–30 Hz	0.0053	0.0062	0.0218
2	5–30 Hz	0.0053	0.0062	0.0217
2	6–30 Hz	0.0053	0.0062	0.0302
2	7–30 Hz	0.0053	0.0062	0.0302
2	8–30 Hz	0.0053	0.0062	0.0302
2	9–30 Hz	0.0053	0.0062	0.0218
2	10–30 Hz	0.0053	0.0062	0.0302
3	1–30 Hz	0.0045	0.0078	0.0078
3	2–30 Hz	0.0047	0.0078	0.0078
3	3–30 Hz	0.0035	0.0129	0.0147
3	4–30 Hz	0.0036	0.0941	0.0941
3	5–30 Hz	0.0032	0.1022	0.1022
3	6–30 Hz	0.0030	0.1153	0.1153
3	7–30 Hz	0.0033	0.0965	0.1012
3	8–30 Hz	0.0028	0.0941	0.0964
3	9–30 Hz	0.0032	0.1215	0.1431
3	10–30 Hz	0.0033	0.1439	0.1439
4	1–30 Hz	0.0012	0.0075	0.0087
4	2–30 Hz	0.0011	0.0098	0.0098
4	3–30 Hz	0.0019	0.0286	0.0820
4	4–30 Hz	0.0013	0.0769	0.1004
4	5–30 Hz	0.0016	0.1319	0.1387
4	6–30 Hz	0.0019	0.4194	0.4369
4	7–30 Hz	0.0019	0.3953	0.4663
4	8–30 Hz	0.0011	0.4651	0.4730
4	9–30 Hz	0.0010	0.4613	0.4694
4	10–30 Hz	0.0009	0.4705	0.4788

below 0.9, that is, the parts close to the singularities which are prone to misestimations. The frequency range of the used part of the curve is between 0.9 and 1.7 Hz. The misfit value is much smaller than in Fig. 3(c), indicating that the data points with very high or low ellipticity values, which have been dismissed for this inversion, are more difficult to fit. Despite the small misfit value, the *T* value of the inversion is not acceptable and the ellipticity curve at frequencies above the trough is badly fitted. Both dispersion curve and velocity profile are badly retrieved as well. The deviation in the dispersion curve around 4.0 Hz suggests that the frequency gap between the SPAC and ellipticity data is too large in this case.

Therefore, in Fig. 3(e), a part of the right flank and a small part beyond the ellipticity trough are inverted, omitting ellipticity values around the trough. The frequency range of the inverted ellipticity data lies between 0.7 and 1.7 and between 2.5 and 4.0 Hz. The inversion has both small misfit and *T* values, indicating that the soil structure is very well retrieved.

The frequency gap of Fig. 3(d) can also be reduced by changing the autocorrelation information. Using the 10-m ring autocorrelation curve instead of the 5-m ring, the frequency content of the SPAC function used in Fig. 3(f) is shifted to lower frequencies. For this inversion, the misfit and *T* values are small, the dispersion curve and the shear wave velocity profile are very well retrieved.

These inversions clearly show that, apart from the ellipticity peak frequency itself, the most important part of the ellipticity curve to measure and invert is the right flank of the peak. It also outlines that the frequency gap between ellipticity and autocorrelation data must not be too large, a result which is indeed not very surprising, and will be discussed in more detail afterwards.

Although the left flank of the ellipticity peak in itself is not important for the inversion, it can be used to fix the peak frequency. Actually, when inverting the right flank of the ellipticity peak only, the peak frequency is badly constrained. It is not a straightforward issue to include this frequency value directly in the inversion, but an inclusion of the left flank helps constraining the peak frequency.

The exact ellipticity values at the close vicinity of the peak or trough can also be omitted. The best results for real data inversions can be expected if the whole right flank is measured accurately. If the frequency ranges of the autocorrelation and ellipticity curves differ too much, additional information beyond the trough frequency can be included for the ellipticity inversion, or a wider autocorrelation measurement layout could be used, if possible. However, beyond the trough frequency, the measured ellipticity is more prone to be affected by higher modes.

Finally, this exercise showed that it is possible to retrieve the shear wave velocity profile down to about 200 m with a seismic array aperture of only 10 m.

2.2.2 Model without a singularity in the ellipticity curve (model B)

Ellipticity curves not showing singularities are often not considered as valuable information contributing to the inversion. At least, the literature examples of ellipticity inversions to retrieve the shallow ground structure are focused on models including singularities (Scherbaum *et al.* 2003; Arai & Tokimatsu 2004, 2005; Parolai *et al.* 2005). In the frequency range interesting for lithospheric structure imaging, however, the used ellipticity curves do not show singularities, but they still contain information valuable for the inversion (Tanimoto & Alvizuri 2006; Yano *et al.* 2009). Here, we will show that ellipticity curves without singularities are also valuable for the retrieval of superficial ground structures.

Model B does not exhibit any ellipticity singularities. The ellipticity curve shows a maximum of 1.71 at 0.73 Hz and a minimum of 0.36 at 9.44 Hz. Its ellipticity peak is broad and exhibits a sort of fine structure which is probably related to the different layer boundaries, but certainly not in a simple way. Fig. 4 shows the results of joint inversions of SPAC and different parts of the ellipticity curve. The misfit and *T* values for the best-fitting model are shown in Table 2. The theoretical SPAC curve for a radius of 5 m was used. Fig. 4(a) shows the inversion of the SPAC information only. Due to the similarity of the SPAC curves, the results are very similar to those of Fig. 3(a). The superficial ground structure is well retrieved, but layers deeper than 50 m are not resolved at all.

In Fig. 4(b), the broad ellipticity plateau between 0.75 and 9.5 Hz was used. The inversion fits the ellipticity curve well, the dispersion curve and the shear wave velocity profile are retrieved. This is also indicated by the low *T* value.

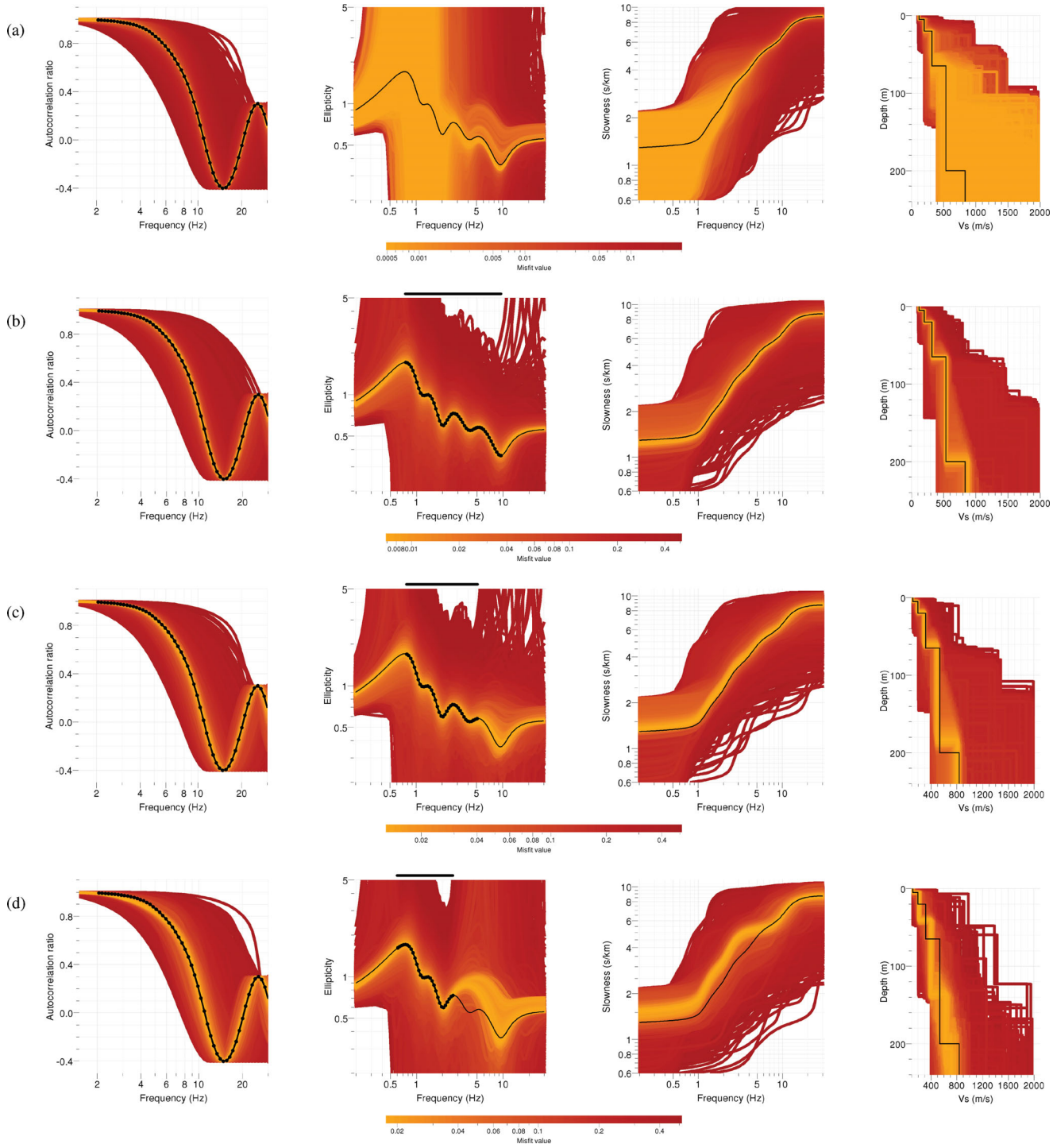

Figure 4. Inversion results for joint inversions of the SPAC curve (left-hand side) and the ellipticity curve (centre left) for the soil structure model without singularities: dispersion curves (centre right) and shear wave velocity profiles (right-hand side). The data points used for the inversion are shown as black dots, the curves corresponding to the true model as solid lines. The black bars above the ellipticity curves indicate the frequency range used for the inversion. (a) Inversion of the SPAC data only. (b–d) Joint inversions of the SPAC and ellipticity data (b) between 0.75 and 9.5 Hz, (c) between 0.75 and 5.2 Hz, (d) between 0.6 and 2.7 Hz.

Using less data, that is, the ellipticity curve between 0.75 and 5.2 Hz, still yields good results (see Fig. 4c). The dispersion curve is well retrieved, but slight uncertainties in the estimation of the shear wave velocity profile can be seen.

However, using the ellipticity values between 0.6 and 2.7 Hz only is not sufficient to find the correct soil structure (Fig. 4d). The ellipticity at higher frequencies is badly estimated and the dispersion curve and velocity profile are badly fitted as well, although the minimum misfit value is in the same order as for the other inversions.

This inversion proves that even in the case of an ellipticity without clear peak or singularities, the ellipticity curve carries important information on the ground structure and can be used to find the soil structure.

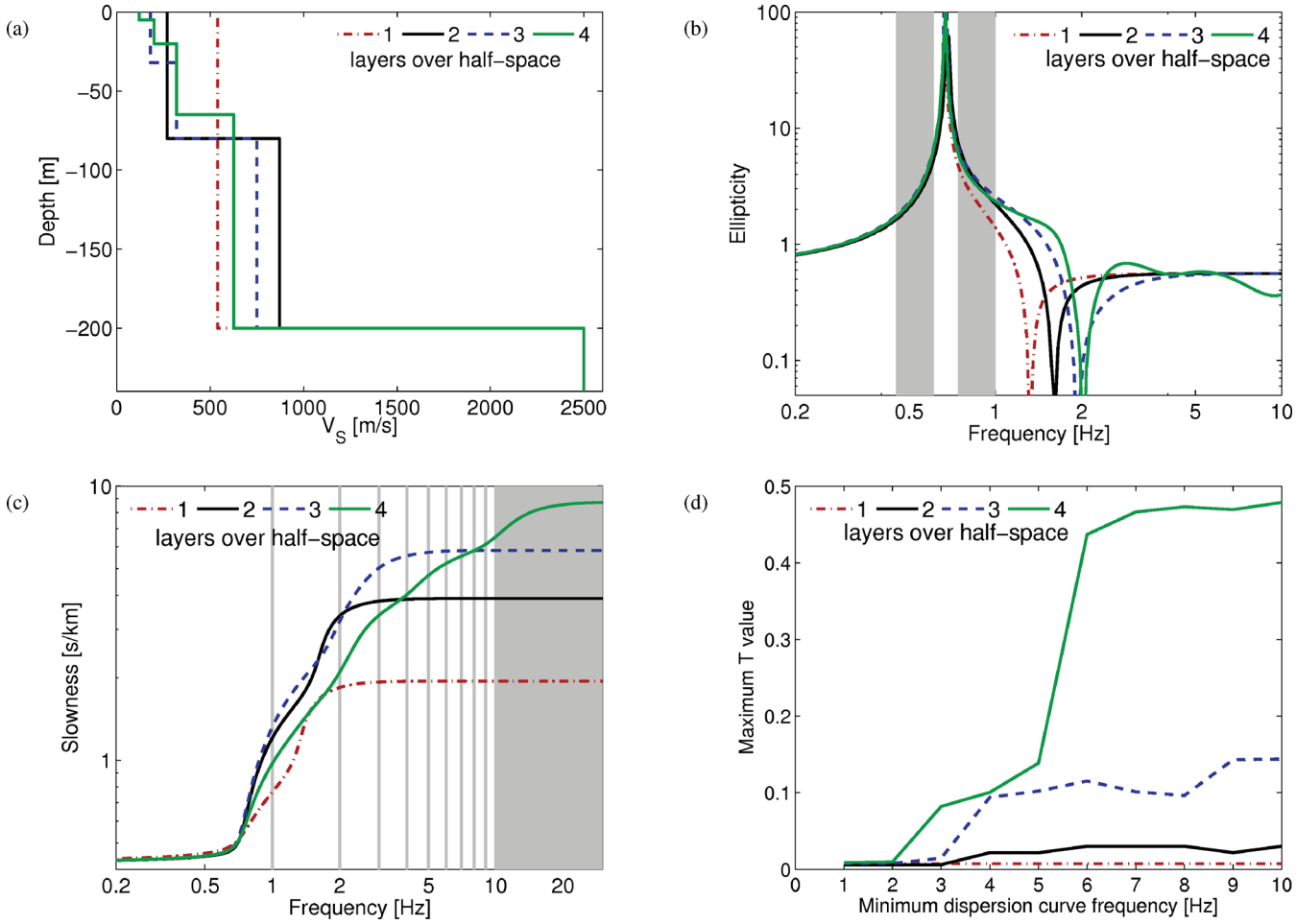

Figure 5. (a) Shear wave velocity profiles of the different models used for the investigation of the influence of the gap between ellipticity and dispersion data on the inversion. (b) The corresponding ellipticity curves, where the gray areas mark the frequency range used for the inversion. (c) The corresponding dispersion curves. In all tests, dispersion data up to 30 Hz were used, but the lower frequency limit changed from 1 to 10 Hz (indicated by the gray lines, the gray area is common to all inversions). (d) Maximum T values of the population of models with misfits less than 1.05 times the minimum misfit value as a function of the frequency gap between the ellipticity and dispersion data. The *x*-axis indicates the lower frequency limit of the dispersion curve, the higher limit is always 30 Hz.

2.2.3 Summary

First, it should be noted that the shear wave velocity of the bedrock is less constrained than the overlying layers for all inversions in the case of singularities in the ellipticity curve, even if the upper structure is very well retrieved. This is related to the penetration depth of the fundamental mode of Rayleigh waves. As the shear wave velocity in the bedrock is much higher than in the overlying sedimentary layers, the fundamental mode Rayleigh waves sample the bedrock only marginally. In that cases, the inversion yields a strong impedance contrast, but the imprecision in the bedrock can easily exceed 20 per cent. If the ellipticity curve does not exhibit singularities, the fundamental mode Rayleigh wave also samples the bedrock structure, resulting in a good constraint on the bedrock velocity in this case.

2.3 Evaluation of the frequency gap between both inverted data

Both inversions of ellipticities including singularities or not have outlined that the frequency gap between the different dispersion data (ellipticity and SPAC curves) should not be too large to ensure good inversion results. However, it is not straightforward to determine the frequency down to which a SPAC curve actually carries information because of the shape of the Bessel function. To better quantify the tolerable frequency gap, we have performed a simple sensitivity study, using dispersion curve data instead of SPAC curves.

Starting with model A, a model with four layers over a continuous half-space, we constructed three other models with one to three layers over half-space, which all exhibit the same ellipticity peak at 0.7 Hz and troughs close to 2.0 Hz (Fig. 5a). The parameters of the different models are given in Table 3. All models have a bedrock depth of 200 m. For each of these models, we inverted the ellipticity curve in the same frequency range, that is, the left flank of the ellipticity peak between 0.45 and 0.61 Hz and the right flank between 0.74 and 1.00 Hz (Fig. 5b), jointly with different parts of the corresponding dispersion curve of the fundamental mode Rayleigh wave (Fig. 5c). The dispersion curves of the different inversions were taken between a lower frequency limit (varying from 1 to 10 Hz) and a higher limit of 30 Hz. For each inversion, we calculated the T values according to eq. (2) in the frequency range from 0.7 to 30 Hz. As the misfit value of the inversion is also based on the ellipticity data, there is a difference between misfit and T values. The inversion is driven towards low misfit values and

the *T* values for all generated models are calculated afterwards. All models with misfit values lower than 1.05 times the minimum misfit are considered as good inversion results and the maximum *T* value in this population of models indicates the integrity of the inversion. In Fig. 5(d), these *T* values are plotted as a function of the lower frequency bound of the dispersion curve for all four models. The parameters of all inversions are given in Table 4.

For the case of a single layer overlying a homogeneous half-space, the dispersion curve is flat above 3 Hz. This means that all the necessary information on the superficial layer is included in any data point above that frequency and that the ellipticity curve is sufficient to constrain the second layer. Therefore, the maximum *T* value is constant for all lower frequency limits for that model. For the two-layer model, the information of the second layer is only included in the dispersion curve below about 3 Hz. This explains why the *T* values increase for this model if the lower limit is larger than 3 Hz. For the three-layer model, the *T* value also increases for lower limits above 3 Hz, but the effect is much stronger than in the previous case. This is certainly linked to the additional layer in this case. Finally, for the four-layer model, the *T* value already increases for lower dispersion curve limits above 2 Hz, and extremely increase for lower bounds over 5 Hz. In that case, the dispersion curve carries too few information on the lower layers to actually be linked to the ellipticity curve.

This study illustrates that it is not possible to actually give a simple rule for the lowest acceptable frequency gap between ellipticity and dispersion (or SPAC) data in joint inversions. The complexity of the soil structure also plays a major role. For a very simple model of a single layer over a half-space, it is actually sufficient to measure the dispersion curve at high frequencies (e.g. using MASW measurements) and to constrain the bedrock with a measurement of the ellipticity peak. The more complex the ground structure model gets, however, the smaller the frequency gap between the different information has to be. Therefore, we recommend to keep the gap as small as possible in real applications if no further information on the actual complexity of the underground is available.

2.4 Inversion of misestimated ellipticity curves

The measurement of ellipticity curves can always be biased by systematic errors, introduced, for example, by a wrong estimation of the amount of Love waves or incomplete elimination of waves other than Rayleigh waves. This section deals with inversion errors introduced by common ellipticity misestimations. In general, any ellipticity estimation technique uses the correlation between vertical and horizontal signals. Therefore, any ellipticity estimation is prone to misestimation at the singularities. However, as Love waves are only present on the horizontal components, this effect is more pronounced at the point where the Rayleigh wave contribution to the horizontal signal vanishes, that is, at the trough. In this section, the same autocorrelation curve as in the previous subsections will be inverted jointly with misestimated ellipticity curves of model A. As in Section 2.2.1, the inversion of the ellipticity curve parts between 0.7 and 1.7 and 2.5 and 4 Hz gave the best results, these parts will be used for the inversion here and the inversion shown in Fig. 3(e) will serve as reference inversion.

2.4.1 Biased ellipticity estimation

Here, we will consider joint inversions of ellipticity curves which are misestimated by a systematic bias. Except for the ellipticity bias, the same information as in Fig. 3(e) has been inverted, that is, the autocorrelation curve for a radius of 5 m between 2 and 30 Hz and the ellipticity information in the ranges 0.7–1.7 and 2.5–4.0 Hz. The systematic ellipticity bias is maximum at 1.7 Hz (e.g., + 25 per cent and + 50 per cent in Fig. 6a and b, respectively) and vanishes at 0.7 Hz, varying linearly between both values. Between 2.5 and 4.0 Hz, the relative ellipticity bias is the same as at 1.7 Hz. In this way, low ellipticity values are more affected by this misestimation than larger ellipticity values. Only the overestimation of ellipticity is meaningful for real data measurements and will be shown in detail. However, we also performed the same exercise for underestimated ellipticity values. It should be noted that, for the reference inversion (Fig. 3 e), the true soil structure model exists and is accessible to the inversion. Therefore, a misfit value of 0 would be possible in the respective inversion. For biased ellipticity curves, however, the existence of a model exhibiting exactly the biased ellipticity curve is rather improbable. Consequently, the minimum misfit values of such inversions are likely to increase when increasing the bias. For overestimated ellipticity curves, this effect is still small with minimum misfits about twice as large as for the reference inversion (compare Tables 2 and 5). For underestimated ellipticity curves, which are not shown here, however, the misfit value even reaches 20 times the reference misfit.

Figs 6(a) and (b) show the results of the inversions for maximum ellipticity overestimations of 25 and 50 per cent, respectively (inversion parameters in Table 5). The superficial structure is mainly controlled by the autocorrelation curve and is quite robust against ellipticity misestimations. Therefore, the deeper parts of the velocity profiles should be mainly affected, corresponding to the low-frequency part of the dispersion curves. For a maximum ellipticity overestimation of 25 per cent (Fig. 6a), the true velocity profile is still well retrieved, whereas for 50 per cent (Fig. 6b), the deeper structure is misestimated, that is, the layer depths and velocities are overestimated. Anyway, the bedrock depth overestimation is still lower than 20 per cent and the low T values indicate that both inversions are still in good agreement with the true model.

In Fig. 7, different values characterizing biased ellipticity inversions are shown: The bedrock depth, the mean velocity of the sedimentary layers and the traveltime between the surface and the bedrock. The mean velocity is the ratio between the bedrock depth and the traveltime. The figure includes negative ellipticity biases as well. The traveltime values vary only slightly and are much smaller than the introduced ellipticity bias. Actually, scaling a given soil structure does not alter the traveltime. Bedrock depth and mean velocity are more affected by ellipticity misestimations, but their variations are still smaller than the introduced ellipticity bias. Negative ellipticity biases introduce larger velocity and depth variations than positive ones. This indicates that joint inversions including ellipticity curves are more robust against the common case of ellipticity overestimation than against the rare case of underestimation.

2.4.2 Trough misidentification

Another form of ellipticity measurement error is the misidentification of the trough frequency. Due to the presence of Love waves, the ellipticity can be overestimated around the trough to such a degree that the measured ellipticity curve does not exhibit a clear trough any more. Such a case is shown in Fig. 6(c), where the same ellipticity information as in Fig. 3(e) is used, but the values between 1.7 and 2.5 Hz are interpolated linearly. The inversion converged more slowly than the other inversions, but after generating 115 100 models, it actually succeeded in finding a soil structure exhibiting a singular peak, but no trough. Despite some deviations, the

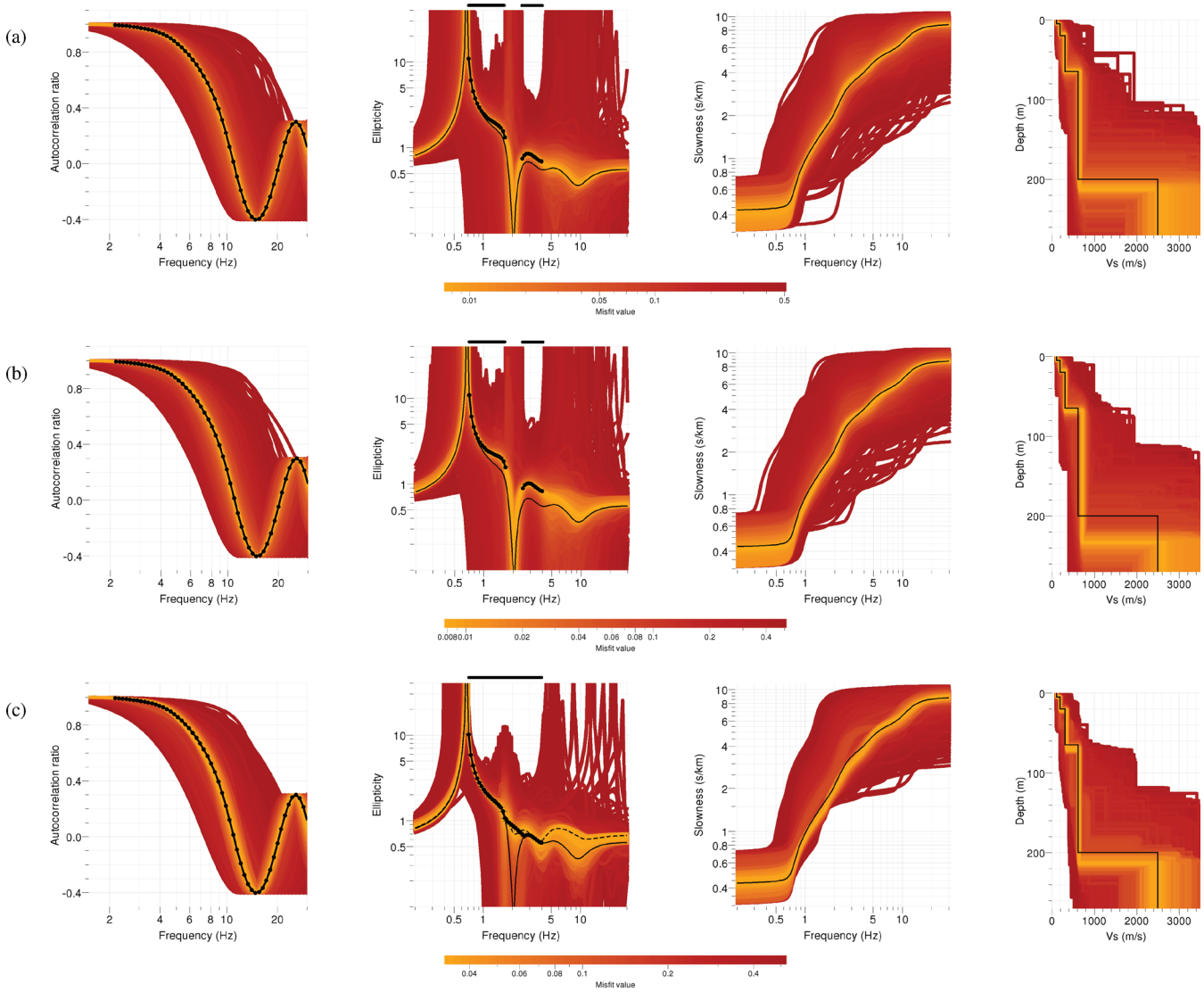

Figure 6. Inversion results for joint inversions of the autocorrelation curve (left-hand side) and biased ellipticity curves (centre left): dispersion curves (centre right) and shear wave velocity profiles (right-hand side). The black dots indicate the data points used for the inversion and the solid lines the corresponding curves for the unbiased model. The black bars above the ellipticity curves indicate the frequency range used for the inversion. The ellipticity curves are biased by maximum (a) +25 per cent, (b) +50 per cent. (c) Inversion of an ellipticity curve between 0.7 and 4.0 Hz, which corresponds to the real curve between 0.7 and 1.7 and between 2.5 and 4.0 Hz and is interpolated in the range between 1.7 and 2.5 Hz. For clarity reasons, the model with lowest misfit value is indicated by the dashed line in the ellipticity plot.

Table 5. Misfit values for the best-fitting models of joint inversions of the autocorrelation curve and misestimated parts of the ellipticity curve of model A. The *T* values for the best-fitting model and the maximum *T* value of all models with misfits lower than 1.05 times the minimum misfit are also indicated.

Figure reference	Autocorrelation curve Array radius	Autocorrelation curve Frequency range	Ellipticity curve	Ellipticity misestimation	Number of models	Minimum misfit	*T* value (0.7–30 Hz) best model	*T* value (0.7–30 Hz) maximum
Fig. 6(a)	5 m	2–30 Hz	0.7–1.7, 2.5–4.0 Hz	+25 per cent maximum	100 100	0.0074	0.026	0.027
Fig. 6(b)	5 m	2–30 Hz	0.7–1.7, 2.5–4.0 Hz	+50 per cent maximum	100 100	0.0080	0.038	0.040
Fig. 6(c)	5 m	2–30 Hz	0.7–4.0 Hz	trough interpolation	115 100	0.0330	0.054	0.055

best model of the inversion is in acceptable agreement with the true model. This means that even a partly biased or misinterpreted ellipticity curve can still be inverted successfully.

2.5 Results

The first part of this paper showed the theoretical possibilities, constraints and limits of inversions including the Rayleigh wave ellipticity to retrieve the local ground structure. First of all, the possibility of inverting an ellipticity curve jointly with an autocorrelation or dispersion curve was shown. The frequency ranges of both measurements do not necessarily have to overlap, but should be as close as possible. In the case of an ellipticity curve with singularities, the ellipticity curve can be truncated to exclude too high or too low values. As the left flank of the ellipticity peak does not carry important information, the important frequency range for

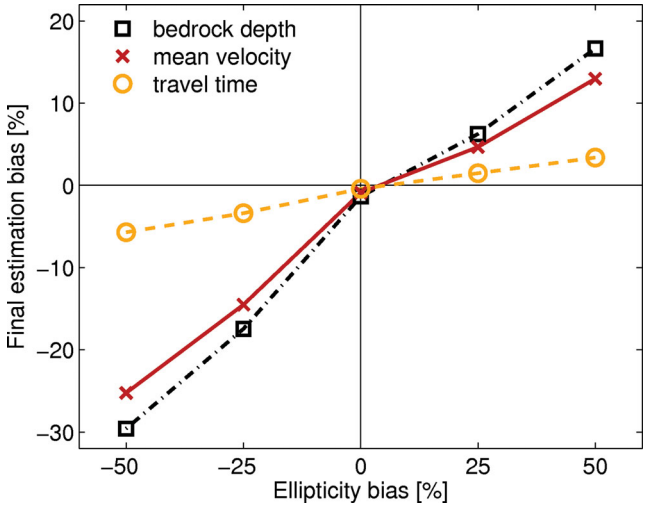

Figure 7. Percental deviation of bedrock depth, mean velocity and shear wave traveltime from the surface to the bedrock in function of the introduced bias on the ellipticity curve. The *x*-axis indicates the maximum ellipticity deviation.

the inversion is above the peak frequency. However, the left flank of the peak should be included for a better constraint of the peak frequency.

If the ellipticity curve does not exhibit singularities, the complete right side of the peak which is, in general, broader than in the previous case has to be included in the inversion. For misestimated ellipticity curves, the induced errors in the soil structure are, in general, smaller than the original misestimation.

In the next part, the lessons learned in the first part will be applied to real data measurements.

3 APPLICATION TO REAL DATA MEASUREMENTS

3.1 Site presentation

The inversion strategy developed above has been applied to data measured during the European NERIES project (Bard *et al.* 2010). During this project, ambient seismic vibrations have been recorded at different European sites, using three to four arrays of different sizes at each site. Each array consisted of a central station surrounded by a more or less perfect ring of seven seismometers. The acquisition system was composed of Earthdata digitizers equipped with 5s-Lennartz three-component sensors. Additional MASW measurements have been performed as well (Endrun & Renalier 2008; Renalier & Endrun 2009). We selected 14 (six in Italy, five in Greece, three in Turkey) out of the 20 sites originally investigated during this project, for which the dispersion curves from array and MASW measurements are in good agreement and could be combined into a single broad-band dispersion curve (from about 1-2 Hz to about 40 Hz) (Di Giulio *et al.* 2012). The locations of these sites are shown in Fig. 8.

The goal of this paper is to retrieve the soil structure using as little information and field effort as possible. Therefore, we will only use the ellipticity obtained at the central station and the autocorrelation curves derived by applying the modified SPAC technique of Bettig et al. (2001) to the smallest array of seismic sensors at each site (or the MASW dispersion curve in the case of Aigio). The apertures of the smallest arrays at the different sites lie between 10 and 30 m. For the Italian and Greek sites, independent borehole measurements (cross-hole or down-hole) are available and can serve as a reference (Picozzi *et al.* 2007). For the Turkish sites (Bolu, Düzce and Sakarya), the reference measurements are former independent inversions of MASW measurements. Borehole measurements give the soil profile at a single point only, whereas broad-band dispersion curve measurements average over a larger part of the structure. Table 6 lists the selected sites and indicates their respective soil classification according to the European EC8 code, the bedrock depth determined by borehole measurements and the size of the smallest seismic array used for the measurements.

3.2 Ellipticity measurements

The ellipticity measurements have been performed using the RayDec technique (Hobiger *et al.* 2009). This method uses the data of a single three-component seismic sensor to retrieve the ellipticity of Rayleigh waves. The algorithm is based on the random decrement technique which is commonly used to characterize the dynamic parameters of buildings or other oscillatory systems. The three-component signal is cut in small time windows starting at the positive zero-crossings of the vertical component. For each time window, the signal of the horizontal components is projected into the direction which maximizes the correlation to the vertical component with a 90° phase shift which is typical of Rayleigh waves. Subsequently, the signals obtained in this way are stacked together and the ratio between the horizontal and vertical motions is estimated by analysing the energy content of the vertical and horizontal stack. To calculate standard deviations for the measurements, the available seismic noise signals are, depending on the signal length, cut into windows of 7 to 10 min. The final ellipticity measurement is then obtained by averaging the RayDec results of these time windows.

Fig. 9 shows the ellipticity curves which were obtained for each station of the smallest array for each site and compares them with the H/V curves for the same sites and the theoretical ellipticity curves derived from the reference measurements. Almost all sites show qualitatively identical ellipticity curves for each seismic sensor indicating that the soil structure does not change significantly over small distances. However, for some sites (e.g. Norcia), the ellipticity curves of the different sensors are identical over a limited frequency range only and differ at other frequencies. The peaks of Aigio and Buia at 1.45 Hz can be identified as artificial peaks and are not related to the soil structure. Qualitatively, some sites exhibit very clear ellipticity peaks (Nestos and Volvi), or even two clearly distinguished peaks like Colfiorito, where it is unclear if the second peak is a very shallow resonance effect linked to the fundamental mode or if it belongs to a mixture of higher Rayleigh wave modes. For other sites, the ellipticity curves show a dominant peak which is not singular (Aigio, Benevento, Buia, Düzce, Korinthos, Norcia and Sakarya). Another set of sites exhibits a rather flat ellipticity curve (Bolu, Forlì and Sturno). For Knidi, no qualitative conclusions can be drawn as stations located in a ring of only 5 m radius exhibit different ellipticity curves.

3.3 Inversion strategy

For some of the sites it is unclear if the peaks are really singular or not or where the broad peak actually lies. Anyhow, we try to apply the lessons learned in the previous section to all of the sites. The main reason for this is that low-velocity zones cannot be identified

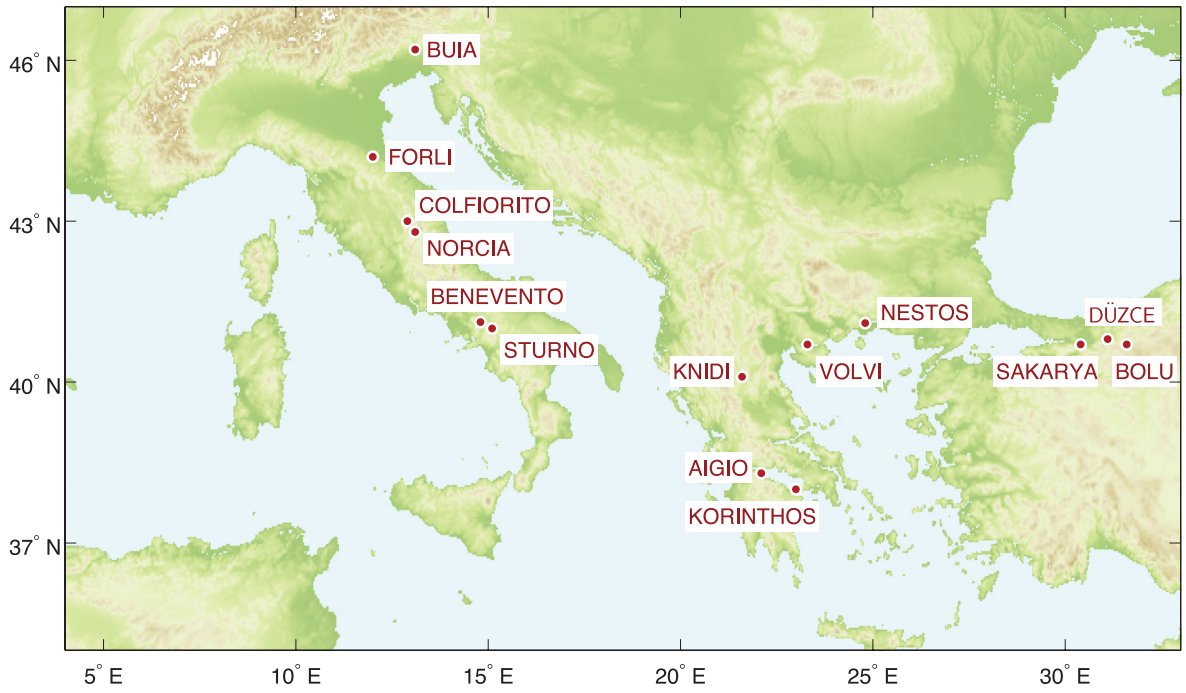

Figure 8. Location of the NERIES sites used in this study.

Table 6. Investigated NERIES sites, including their respective classification according to the European EC8 code, the borehole depth and the bedrock depth determined by borehole measurements (Picozzi *et al.* 2007)[N/A indicates that no borehole measurements are available or that the borehole did not reach the bedrock]. The radius of the smallest array of seismic sensors used in this study is also indicated.

Site	Country	EC8 category	Borehole depth (m)	Bedrock depth (m)	Smallest array radius (m)
Aigio	Greece	B	28	20	not used
Benevento	Italy	B	98	N/A	7.14–9.48
Bolu	Turkey	C	N/A	N/A	7.56–9.29
Buia	Italy	C	52	48	9.32–11.50
Colfiorito	Italy	D	66	55	12.79–16.00
Düzce	Turkey	C	N/A	N/A	8.01–8.83
Forlì	Italy	C	55	N/A	7.41–9.35
Knidi	Greece	E	21	16	7.13–8.59
Korinthos	Greece	C	40	N/A	9.41–10.44
Nestos	Greece	C	64	N/A	6.59–7.24
Norcia	Italy	B	60	N/A	8.67–9.97
Sakarya	Turkey	B	N/A	N/A	11.83–13.67
Sturno	Italy	B	N/A	N/A	8.15–8.77
Volvi	Greece	C	200	196	10.42–13.23

in the ellipticity or SPAC curves. For the sake of simplicity, we deliberately do not introduce constraints from borehole data. This may in case of low-velocity zones or high complexity in the ground structure lead to 'simplified' ground structures. Therefore, we prefer to compare our results to the available broad-band dispersion curves.

We used the following strategy for the inversions: The SPAC curves can be inverted without ellipticity values to get a first idea of the shallow structure, but this is not crucial for a successful inversion. Following the conclusions of the theoretical part, the frequency range of the ellipticity curves used for the inversion depends on whether clear peaks can be seen in the ellipticity curve or not. If a singular peak can be seen, we will use its right flank for the inversion, omitting very high (above 3) and very low (below 0.5) ellipticity values. By inverting the right flank only, the frequency peak is poorly constrained. Therefore, the left flank of the ellipticity peak is included, taking a range of ellipticity values similar to the ones describing the right flank. If the ellipticity curve does not exhibit singularities, the whole peak or plateau part is inverted. If the frequency ranges of the autocorrelation and ellipticity curves differ too much, a larger layout for the autocorrelation measurements is included.

3.4 Integrity of the inversion results

Similarly to the inversion of theoretical ellipticities, the inversion results will be quantitatively compared to the broad-band dispersion curve obtained during the NERIES project. In fact, it would be possible to compare the inversion results to the borehole shear wave profiles. However, we do not have information about the integrity of these measurements or their uncertainties. Moreover, half of the borehole measurements did not even reach the seismic bedrock

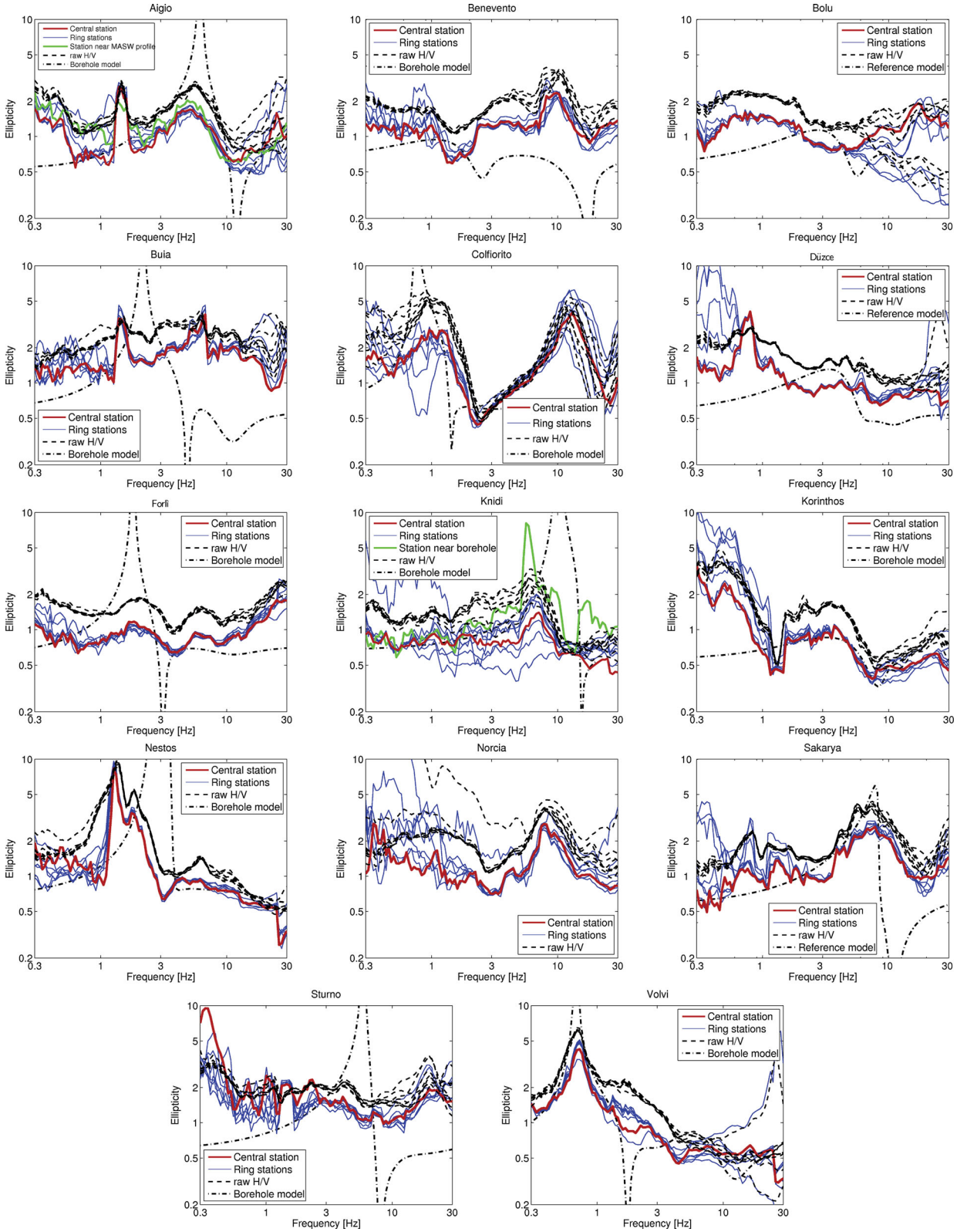

Figure 9. Overview of the ellipticity curves measured with the RayDec technique for the stations of the smallest array for each site. For comparison reasons, the corresponding raw H/V curves are shown as well as the ellipticity curve for the reference measurements. For the sake of clarity, standard deviations are not shown. For Norcia, the low velocity zones of the borehole model did not allow the calculation of a theoretical ellipticity curve.

(Table 8), so we prefer the comparison with the broad-band dispersion curve measurements.

In analogy to the definition of the T value in eq. (2), we define a proximity value which takes into account the measurement errors of the dispersion curves by

$$P = \sqrt{\frac{1}{N}\sum_{i=1}^{N}\left(\frac{s_{\mathrm{meas}}(f_i) - s_{\mathrm{inv}}(f_i)}{\sigma(f_i)}\right)^2}. \quad (3)$$

Here, $s_{\mathrm{inv}}(f)$ indicates the dispersion curve for an inverted model and $s_{\mathrm{meas}}(f)$ the dispersion curve of the direct measurements with error bars $\sigma(f)$, both expressed in terms of slowness. The comparison should range the same frequencies as the measured dispersion curve. In this way, P corresponds to the misfit value the profile would have if we had inverted the dispersion curve. For a model whose dispersion curve lies within the error bars at all frequencies, the P value will be less than 1. Therefore, we will accept inversions with P values below 1. As models which fit the ellipticity data in a comparable way can correspond to different dispersion curves and therefore different P values, it would be arbitrary to calculate the P value only for the model with the smallest misfit value. Therefore, we will calculate the P values for every model generated during the inversion process and indicate the maximum P value for the models whose misfit values are not more than 5 per cent larger than the minimum misfit value, as an upper bound of integrity.

We cannot show the inversions performed for each site in detail here. Therefore, we will only show the inversions for Volvi as an example for an ellipticity curve exhibiting singularities and Aigio as an example without singularities and give an overview of the results for the other sites. The detailed results of these sites are given in the Supporting Information. For the inversions, the ground structures have been parameterized as two to four homogeneous layers overlying a homogeneous half-space, as recommended in Di Giulio *et al.* (2012). For all sites, we started with an inversion with four layers, reducing the complexity if the inversion showed that a layer was not necessary. In this way, models with lower complexity were privileged. Furthermore, we did not allow low-velocity zones in the inversion process.

3.5 Volvi

The Euroseistest site located in Volvi, Greece, is a well-studied test site for seismic measurements (Raptakis *et al.* 1998). The maximum depth of the sedimentary fillings reaches 200 m. For the analysis presented here, we used the smallest array of sensors of the NERIES measurements. The relative positions of the individual sensors are shown in Fig. 10(a). Using these measurements, we can calculate SPAC curves for distances between 10.42 and 13.23 m (seven station pairs fulfill this condition) and between 26.12 and 29.06 m (eight station pairs). A total of 45 min of seismic noise recordings have been analysed. The corresponding SPAC curves are shown in Fig. 10(b) with their respective measurement errors.

The ellipticity curves for all seismic stations of the array are shown in Fig. 9 (bottom right-hand side). All curves exhibit a clear ellipticity peak at 0.73 Hz. The trough frequency seems to be at 4.35 Hz, but an ellipticity value of 0.5 would still be quite large for the trough. The ellipticity for the borehole model is quite similar to the measurements around the peak frequency, but has a trough at 1.76 Hz. At higher frequencies, the measured curves are comparable to the borehole model. Fig. 10(c) shows the ellipticity curve for the central station which was obtained by cutting the signal into five pieces of 9 min each, applying RayDec to all of them and averaging the resulting curves. The averaging generates error bars as well. According to the previously defined inversion strategy, we disregarded ellipticity values above 3. Beyond 1.25 Hz, the error bars are relatively large, suggesting that the ellipticity estimation is unstable at that frequency. The same instability can be seen in Fig. 9 for the seismic stations on the ring. Therefore, we chose to limit the data on the right flank of the peak used for the inversion to frequencies between 0.82 and 1.25 Hz and included the left flank between 0.40 and 0.62 Hz to constrain the frequency of the ellipticity peak.

A first inversion of both SPAC measurements without ellipticity data (Fig. 11 a) constrains the superficial layers down to about 40 m only. The deeper structure is not constrained at all. This can also be seen in the resulting dispersion curves, which fit the direct measurement in a good way for frequencies above 5 Hz. Two other inversions which are not shown here, one of the smaller and one of the larger SPAC curve, are naturally not better than the joint inversion. The parameters of all inversions are given in Table 7.

The next inversions include the ellipticity data shown in Fig. 10(c) with the different SPAC measurements. In the first case, only the small SPAC measurement between 2.7 and 20.0 Hz is included (Fig. 11b). The very superficial structure is well constrained by the SPAC information, and the measured dispersion curve is well fitted at high and low frequencies. In the intermediate range between 2 and 4 Hz, however, the inversion's dispersion curves deviate considerably from the measured curve. This can be explained by the large frequency gap between the ellipticity data (below 1.25 Hz) and the SPAC data (above 2.7 Hz).

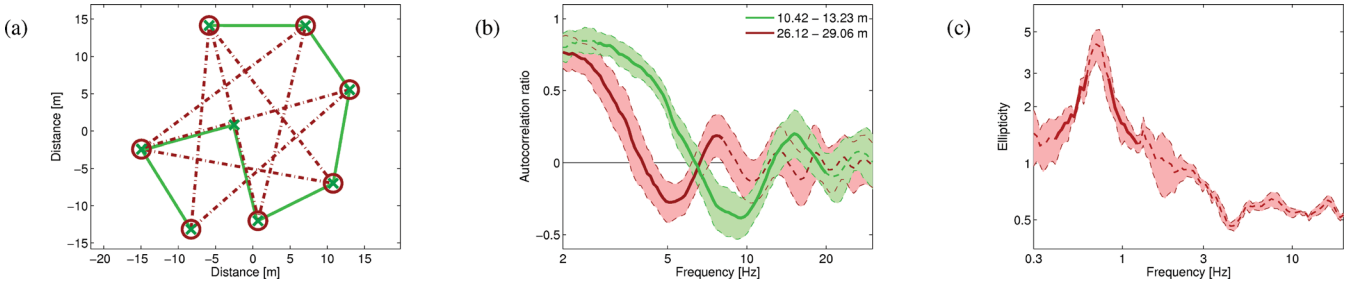

Figure 10. Measurements used for the Volvi inversion: (a) Layout of the seismic sensor array used for the study of Volvi. The station pairs contributing to the spatial autocorrelation curves for the smaller distance case (seven pairs with distances between 10.42 and 13.23 m) and the larger distance case (eight pairs with distances between 26.12 and 29.06 m) are indicated by the solid and dashed lines, respectively. (b) SPAC curves for both cases (frequency ranges: 2.7–20.0 Hz for small SPAC, 2.0–8.0 Hz for large SPAC). (c) Mean ellipticity and standard deviation obtained by averaging the RayDec results for five time windows of 9 min of the central station signal. Used for the inversions: the left flank (0.40–0.62 Hz) and the right flank (0.82–1.25 Hz) of the ellipticity peak. In all figures, the shaded areas indicate the measurement errors and the bold parts were used for the inversions.

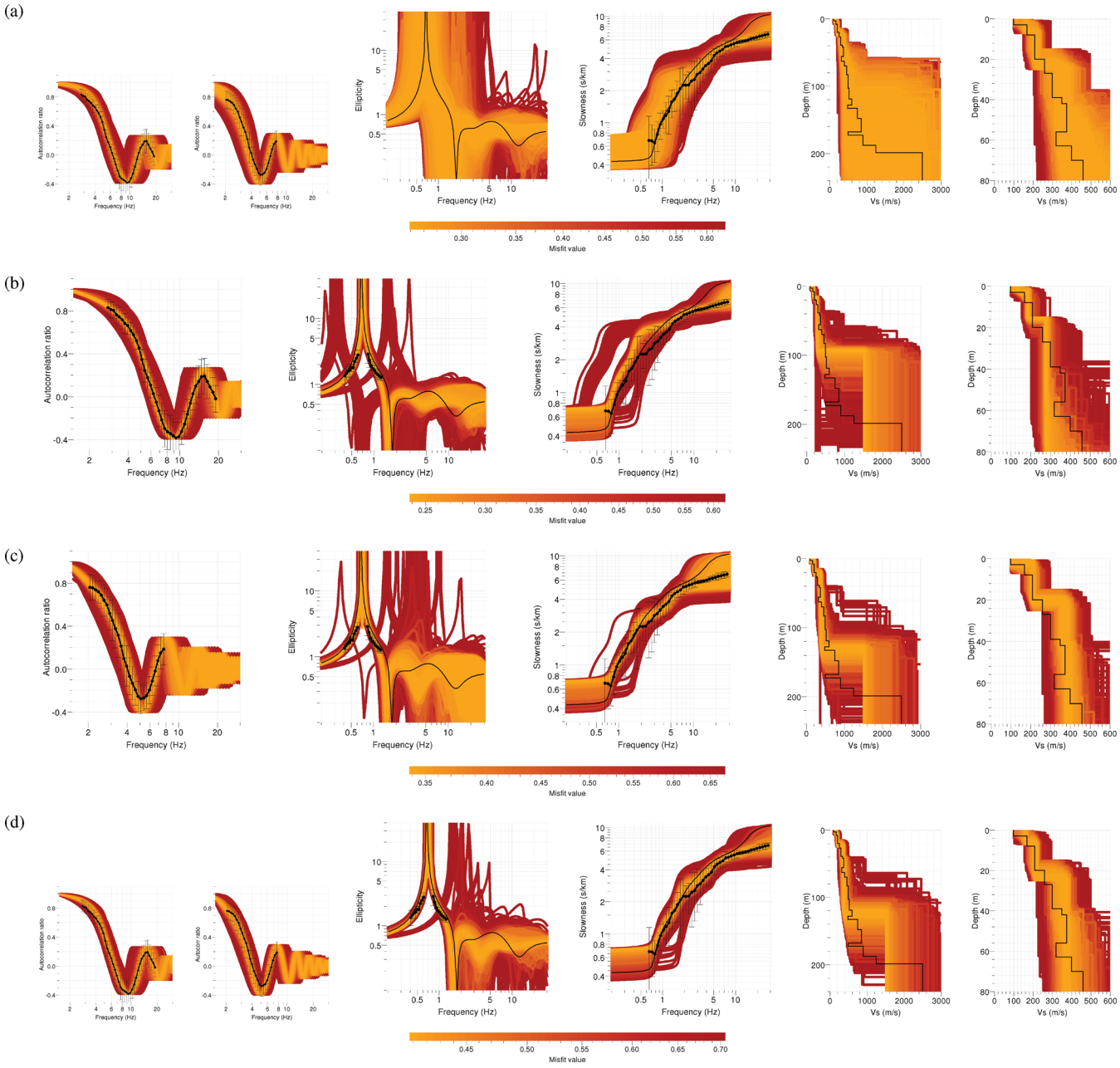

Figure 11. Results for joint inversions of the autocorrelation curve (left-hand side) and ellipticity curve (centre left) for the Volvi data set. Dispersion curve (centre, with dispersion curve data from array measurements) and shear wave velocity profiles (centre right, zoom on the shallow layers on the right) are shown for the models generated in the inversion: (a) using the small SPAC (10.42–13.23 m) and the larger SPAC (26.12–29.06 m) without ellipticity data, (b) using the small SPAC and ellipticity data, (c) using the larger SPAC and ellipticity data, (d) using both SPAC and the ellipticity information. In all figures, the black dots indicate the data points used for the inversion and the solid lines the curves of the borehole model.

Table 7. Misfit and *P* values for the best-fitting models of joint inversions of autocorrelation and ellipticity curves for the Volvi data set. In all inversions, a total of 100 100 models consisting of 4 homogeneous layers overlying a half-space have been generated. See Fig. 10 for the measured data and 11 for the inversions. The maximum *P* values correspond to the largest *P* values of all models with misfits lower than 1.05 times the minimum misfit of the respective inversion.

Figure reference	Inverted data			Minimum misfit	*P* value (0.65 –28.0 Hz)		*P* value for alternative frequency range		
	Small SPAC	Large SPAC	Ellipticity		Best model	Maximum	Frequency range	Best model	Maximum
–	x	–	–	0.11	4.53	4.60	4.0–28.0 Hz	0.48	0.67
–	–	x	-	0.20	1.84	4.83	2.0–8.0 Hz	0.27	0.37
Fig. 11(a)	x	x	-	0.26	0.74	1.49	4.0–28.0 Hz	0.46	0.91
Fig. 11(b)	x	–	x	0.24	0.96	1.21	4.0–28.0 Hz	0.45	1.22
Fig. 11(c)	–	x	x	0.34	1.56	4.16	0.65–8.0 Hz	0.32	0.40
Fig. 11(d)	x	x	x	0.41	0.45	0.79	–	–	–

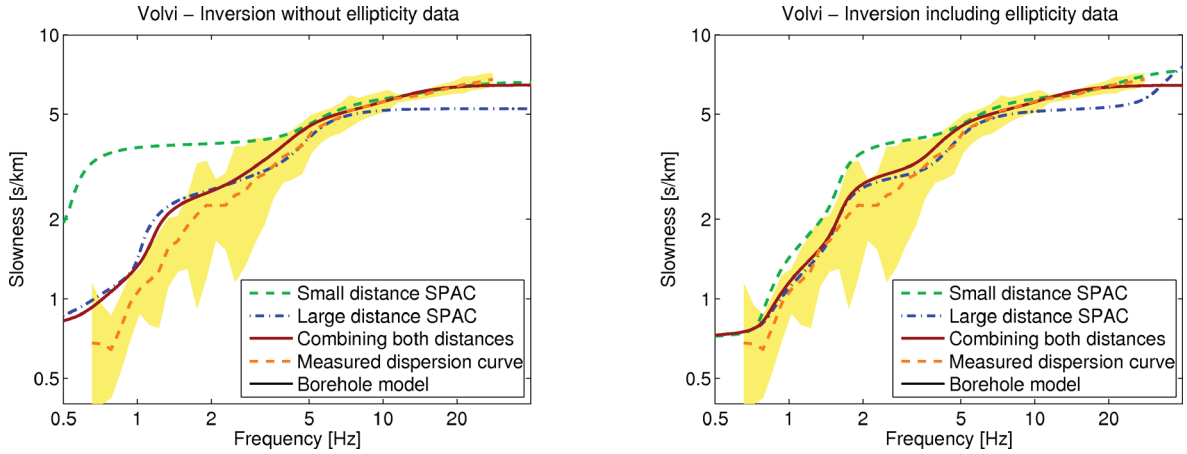

Figure 12. Dispersion curves for the inversions of the Volvi data set without (left-hand side) and including (right-hand side) the ellipticity data: The results for the best models resulting from joint inversions of ellipticity and autocorrelation curves are compared with the measured dispersion curve (shaded area indicates error region) and the reference curve.

Using the larger SPAC layout (between 2.0 and 8.0 Hz) reduces this frequency gap (Fig. 11c). The dispersion curves resulting from the inversion are now in good agreement with the measured one below 10 Hz and the velocity profile is retrieved down to larger depths (bedrock depth situated at 130 m compared to less than 100 m in the previous case). Nevertheless, the shallow velocity profile is badly constrained and the dispersion curves differ for frequencies above 8 Hz.

The last inversion (Fig. 11d) shows the results for using both SPAC data. In this case, the dispersion curve is well fitted over the whole frequency range. However, the resulting bedrock depth still disagrees with the borehole's bedrock depth (200 m), although the upper layers are in good agreement. Nevertheless, an inversion of the direct dispersion curve measurement (between 0.65 and 28.0 Hz) does not yield much different results than our inversion (Di Giulio *et al.* 2012), as both dispersion curves are in very good agreement.

It would require a more detailed and specific investigation to explain the discrepancy between the borehole measurements and the inverted profiles, which is beyond the scope of this paper.

The dispersion curves of all inversions for the Volvi data set are compared in Fig. 12, facing inversions without ellipticity data and inversions including ellipticity data. The benefit of including the ellipticity information is evident for each inversion. Although each inversion yields results which are in agreement with the measured dispersion curve at certain frequencies, an agreement over the whole frequency range can only be achieved by combining both SPAC measurements with the ellipticity curve.

3.6 Aigio

At Aigio, the array layout of the smallest ring was not well suited for small-scale SPAC measurements. Instead, as the ellipticity peak at about 5 Hz is at sufficiently high frequency, we use the dispersion curve obtained by MASW measurements. This dispersion curve is shown in Fig. 13(a). The ellipticity curve (Fig. 13b) was measured by the seismic station which was closest to the MASW profile. It is the mean curve for six 10-min time windows of seismic noise recordings. Calculating the apparent damping of the signal (Dunand 2005) at 1.45 Hz identified the artificial origin of this peak. Therefore, we identify the broad peak with an amplitude of 2 around 5 Hz as the fundamental peak. As the peak is not singular, the complete peak between 3.4 and 10.5 Hz is included in the inversion.

The misfit and P values of the joint inversion of the dispersion and ellipticity data are given in Table 8, the inversion results are shown in Fig. 13(c). The inversion's best model shows some differences to the borehole profile. The latter exhibits a zone of faster velocities at depths between 60 and 120 m with lower velocities below. Such a feature cannot be seen in the MASW and ellipticity measurements and can therefore not be retrieved by our inversion. Furthermore, the borehole profile exhibits an ellipticity singularity, which is not supported at all by the ellipticity measurements. In Fig. 13(d), the resulting dispersion curve for the best-fitting model is compared to the borehole model dispersion curve and the measured dispersion curve. Above 10 Hz, the curves are in good agreement. Below this frequency, the measured dispersion curve is in better agreement with the first harmonic than the fundamental mode of the inversion's best model, even if the fundamental mode is still inside the error bars of the measurement.

3.7 Inversion results for the other sites

In the Supporting Information, the inversions for the 12 remaining sites are shown in detail. The resulting dispersion curves of the best-fitting models are compared with the borehole model dispersion curves as well as the direct dispersion curve measurements for all sites in Fig. 14. The parameters of the respective inversions, among them the P values, are given in Table 1 of the Supporting Information. Except for Forlì, P values below 1 could be found for all sites. For Buia, Knidi, Norcia and Sakarya, this can only be achieved by excluding areas of high frequency (above 20 Hz, see Table 1 of the Supporting Information for details) from the comparison. These frequencies are constrained by the very superficial layers only, which are not well constrained by the data used for the inversion. An autocorrelation curve which has its first root around 10 Hz does not include sufficient information on the shallowest layers. By including higher frequency measurements, for example MASW, in the inversion, these superficial layers could be constrained in a better way.

Consequently, it cannot be expected that our inversions fit the dispersion curve measurements at high frequencies and this part should not be compared. When neglecting high frequencies, a good agreement between the inversions and the direct measurements is obtained for Benevento, Buia, Norcia, Sakarya and Sturno. For Bolu, Düzce and Korinthos, the fundamental mode resulting from

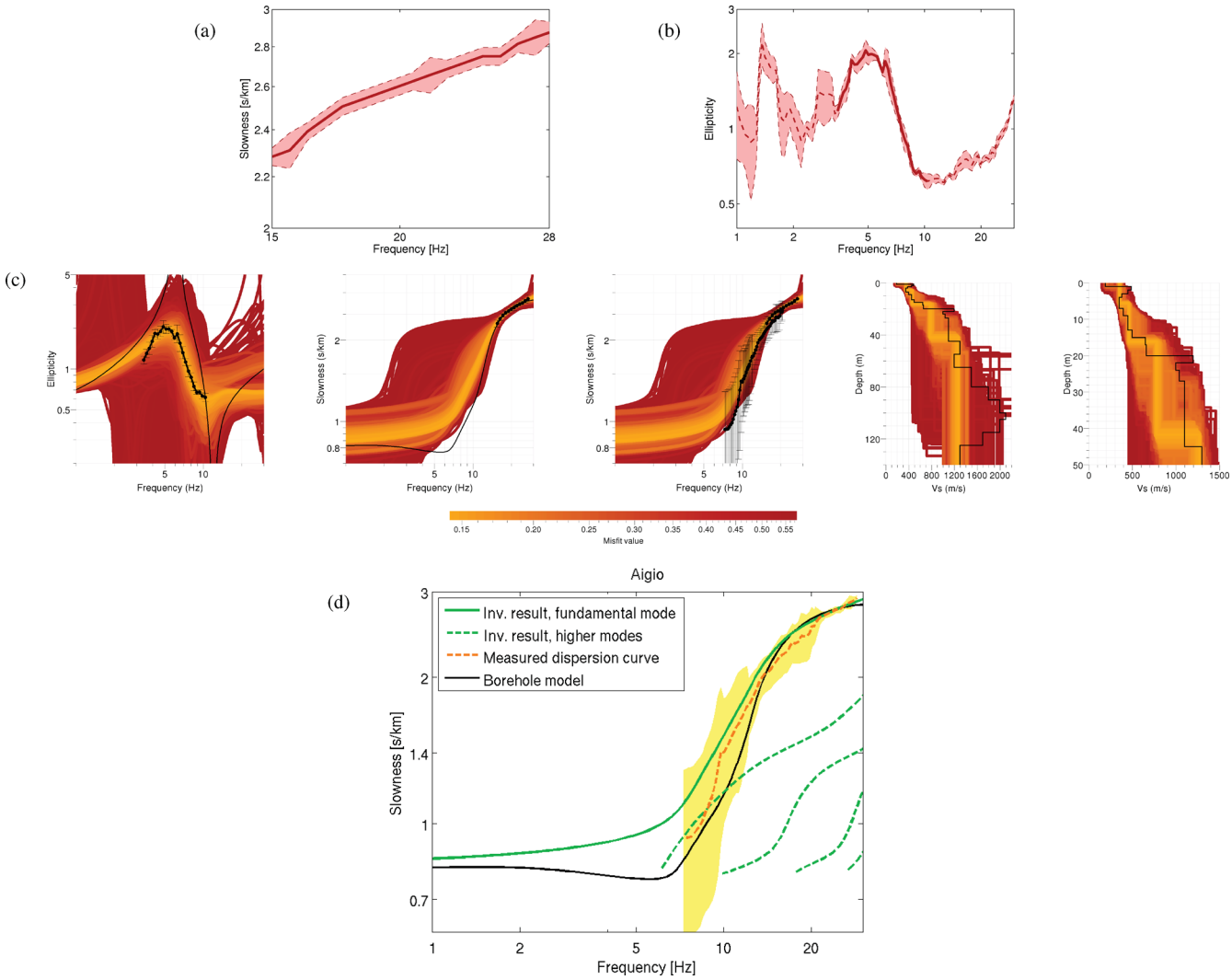

Figure 13. (a–b) Measurements used for the Aigio inversion: (a) Dispersion curve obtained by MASW measurements. (b) Mean ellipticity and standard deviation obtained by averaging the RayDec results for six 10-min time windows of the signal of the station next to the MASW measurements. The shaded areas indicate the measurement errors and the bold parts were used for the inversions. (c) Result for joint inversion of the ellipticity curve (left-hand side, with data points) and dispersion curve (centre left: data points with borehole model, centre: with dispersion curve data from array measurements) for the Aigio data set. The resulting shear wave velocity profiles are shown on the right (centre right: velocity profiles, right: zoom on the superficial 40 m). In all figures, the black dots indicate the data points used for the inversion and the black lines the curves of the borehole model. (d) Dispersion curves for the inversions of the Aigio data set: The results for the best models resulting from the inversion in (c) are compared with the measured dispersion curve (shaded area indicates error region) and the reference curve.

Table 8. Misfit and *P* values for the best-fitting models of joint inversions of dispersion and ellipticity curves for the Aigio data set. See Fig. 13 for the measured data and the inversion. The maximum *P* value corresponds to the largest *P* value of all models with misfits lower than 1.05 times the minimum misfit.

Figure reference	Dispersion curve	Ellipticity curve	Layers over half-space	Number of models	Minimum misfit	*P* value (7.3–28.5 Hz) Best model	Maximum
Fig. 13(c)	15–28 Hz	3.4–10.5 Hz	3	100 100	0.14	0.52	0.55

the inversions and the direct measurements diverge at frequencies below 5 Hz. However, a look at the higher modes of the best model suggests that the direct measurement at these frequencies corresponds to the first harmonic mode rather than the fundamental one. Since the peak of the ellipticity is mostly dominated by the fundamental mode Rayleigh wave, the inversion of ellipticity curves can help in the modal interpretation of a measured dispersion curve, a critical and difficult task in surface wave inversion (e.g. Xia *et al.* 2003; O'Neill & Matsuoka 2005; Cornou *et al.* 2009).

At Colfiorito and Nestos, the inversions are in good agreement with the direct measurement over the whole frequency range. For Knidi, a comparison of the ellipticities of the individual sensors (see Fig. 9) already indicated that the site is quite inhomogeneous and that special attention has to be paid for the inversion of ellipticity data. In contrast to the station near the borehole (about 40 m west of the array), the stations of the smallest array do not show a singular ellipticity peak. Consequently, the inversion results depend on the used ellipticity curve. Using the ellipticity with

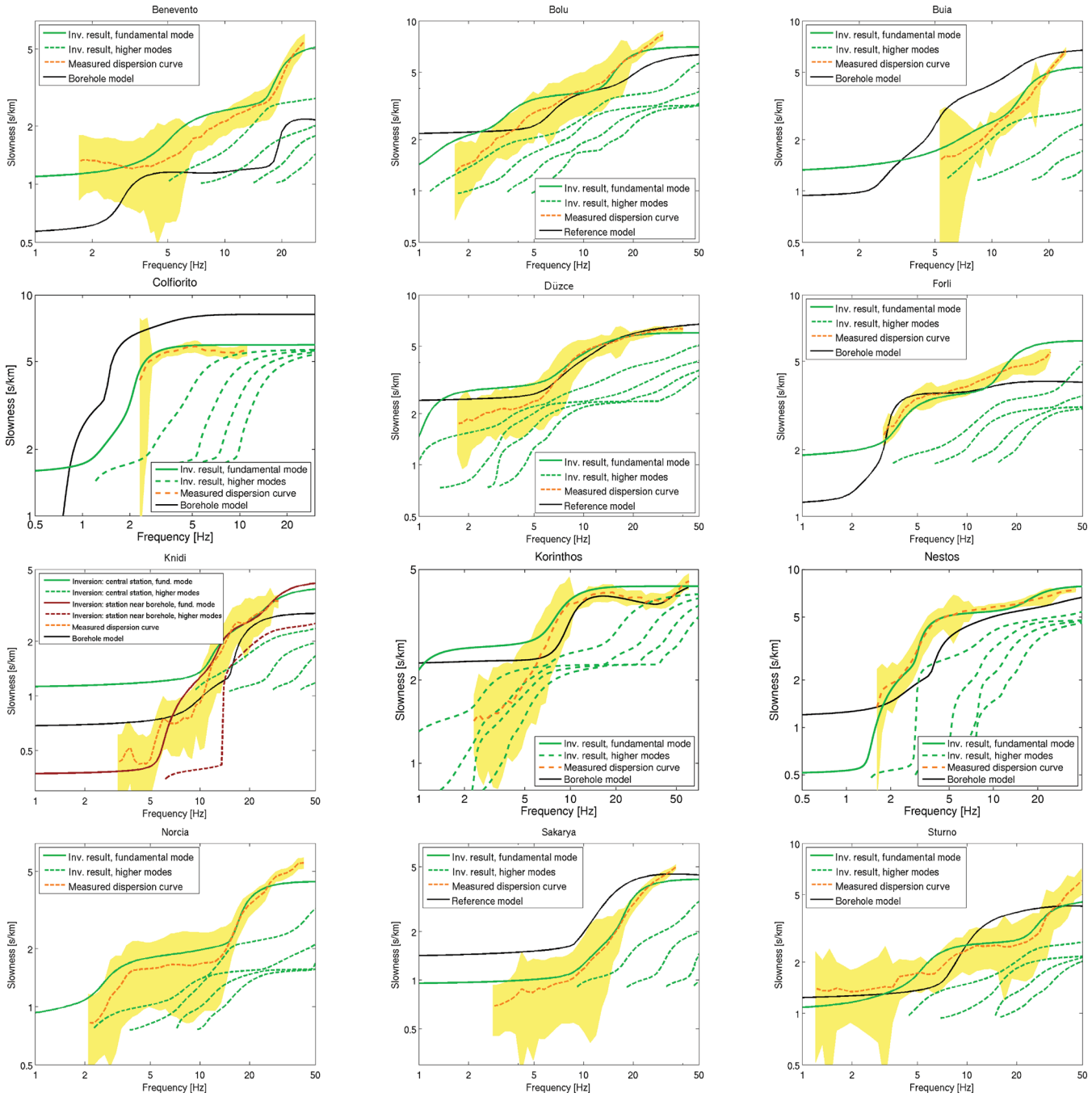

Figure 14. Overview of the dispersion curves for all sites: The results for the best models resulting from joint inversions of ellipticity and autocorrelation curves are compared with the measured dispersion curves (shaded areas indicate error regions) and the reference curves.

singularity is in better agreement with the measured dispersion curve.

3.8 Overview of the results for all 14 sites

Fig. 15 shows the percental differences between the directly measured dispersion curves and the ones resulting from the ellipticity inversions. Only the dispersion curves for the respective models with lowest misfit values are shown. All dispersion curves have been transformed in the wavelength domain before comparison. For Bolu, Düzce and Korinthos, where the inversion results indicate that the measured dispersion curve belongs to different modes, the comparison is shown for the inversion's mode which is closest to the direct measurement. This explains the jumps in the respective curves.

For wavelengths between 10 and 100 m, the differences between both dispersion curves do not exceed 10 per cent for most of the sites. At wavelengths below 10 and above 100 m, the differences between direct measurements and inversions are larger. As already mentioned, short wavelengths correspond to the very superficial structure, which is not well constrained by the used autocorrelation measurements and might be constrained in a better way by active MASW measurements. Such measurements are included in the directly measured dispersion curves. For large wavelengths,

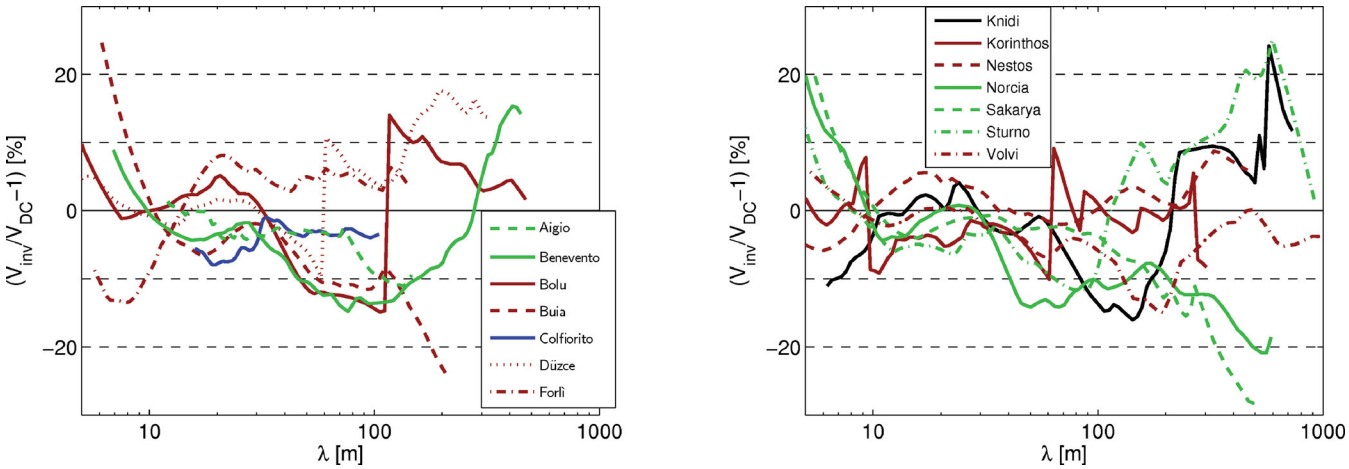

Figure 15. Comparison of the percental differences between the dispersion curves of the best-fitting models resulting from the joint inversions of ellipticity and autocorrelation curves with the directly measured dispersion curves for all analysed sites.

the bedrock velocity influences the dispersion curves. As has been shown in the section on the theoretical aspects of ellipticity inversions, this parameter is badly constrained by the ellipticity curve. A loss of agreement to the direct measurements at these wavelengths is therefore not surprising.

4 DISCUSSION

The first part of this paper dealt with the inversion of theoretical ellipticity and autocorrelation curves. We first showed that additionally to the peak frequency itself the right flank of the ellipticity peak carries the important information on the soil structure for ellipticity curves exhibiting singularities. However, the left flank may also be included in any inversion to better constrain the peak frequency. A further important result is that the ellipticity values just around the singularities, peak and trough, can be omitted without negative influence on the results. This means that the ellipticity curve can be truncated at high and low values. Actually, any estimation of ellipticity depends on the correlation of vertical and horizontal components. As one of both components vanishes at the singularities, the estimation at these points gets biased by the presence of Love or body waves or additional instrumental noise. Therefore, it is an advantage that these data points are not necessary for successful inversions. For ellipticity curves without singularities, this problem does not exist and the complete measured peak should be used in the inversion. Another important result is that such ellipticity curves also carry important information on the soil structure.

As an ellipticity curve can never be inverted without additional information, it is questionable which additional information should be used. SPAC measurements are rather well suited for this task, but MASW measurements can also be used if the ellipticity peak occurs at high frequency. We showed that a frequency gap between both information may be allowed. While a large gap may provide suitable inversion results for simple structures, it may lead to clearly biased inversion estimates for more complex structures. It is difficult to give an exact rule for the frequency gap. For Volvi, a site with a complex structure, a factor of 2.16 was too large, while a factor of 1.6 was small enough. For practical uses and without any prior information on the complexity of the ground structure, we thus recommend that a factor of 2 should in any case not be exceeded to stay on the safe side. Consequently, the interstation distance used for the SPAC measurements should be chosen as small as possible for a good resolution of the superficial layers, but at the same time as large as necessary to assure a good link to the ellipticity curve. To estimate the array size needed for the autocorrelation measurements, preliminary information on the underground structure has to be known or a first ellipticity measurement could indicate the ellipticity peak frequency.

The second part of the paper was dedicated to the application to real data measurements at 14 different European sites (shallow to deep and soft to stiff sites). Although we did not allow low-velocity zones in the inversion and interpreted all ellipticity curves as fundamental mode curves, we found very good agreement (relative deviation below 10 per cent) for all sites between the measured broad-band dispersion curves and the dispersion curves obtained through joint inversion of ellipticity and high frequency dispersion SPAC or MASW data. Such ellipticity inversions thus present an interesting alternative to the deployment of several arrays of different sizes to investigate the ground structure. Furthermore, at some sites, the ellipticity inversions have been shown to help in identifying the fundamental and harmonic Rayleigh wave mode branches of the measured broad-band dispersion curve. For Buia, Düzce and Korinthos (and Aigio), the ellipticity curve inversions suggest that, at low frequencies, the directly measured dispersion curves are indeed dominated by the first or second harmonic mode.

5 CONCLUSION

We made a systematic study of the estimation of shear wave velocity structures by joint inversions of Rayleigh wave ellipticity and SPAC or MASW measurements. The results of the theoretical study outlined that for ellipticity curves with singularities the right flank of the ellipticity peak together with the peak frequency contain the important information on the soil structure. The left flank can be included in the inversion to better constrain the peak frequency. For ellipticity curves without singularities, the whole area of the broad peak should be inverted if such a peak exists.

These inversion rules have been successfully applied to real data examples in the second part of the paper. Although possible low-velocity zones were not allowed in our inversions and we assumed that the fundamental Rayleigh wave mode dominates over the

frequency range encompassing the right flank of the ellipticity, we found a very good agreement between dispersion curves computed from the inverted shear wave velocity structure and directly measured broad-band dispersion curves at the same sites. Furthermore, the inversion of ellipticity data may be helpful in the mode identification of the dispersion curves.

In comparison to the measurement of broad-band dispersion curves by means of noise array recordings using several array layouts, the approach presented in this paper requires less effort. The measurements can be carried out faster and the computational effort is small. Anyhow, the field effort might still be reduced by using less seismic stations for the SPAC measurements. On the one hand, Okada (2006) showed that an array layout with three equally spaced ring stations surrounding a central station is sufficient to retrieve the correct SPAC curve below the first minimum of the Bessel function for any noise source distribution. On the other hand, Morikawa *et al.* (2004) suggested a method using only two seismic stations to perform SPAC measurements (2s-SPAC). Using this method, the reference station is fixed while the second station changes its position during the measurement. This method assumes that the seismic noise wavefield is stationary in time. In any case, even with a larger number of seismic sensors, small-scale ambient vibration array measurements can be carried out very fast, with measuring times of less than 1 hr. Therefore, at least for soft sites, the presented method can be very helpful for extensive site characterization.

ACKNOWLEDGMENTS

We would like to thank all those who helped to perform the measurements: Mehmet Akif Alkan, Marios Anthimidis, Stéphane Drouet, Markus Gurk, Yıldız İravul, Ioannis Kalogeras, Andreas Köhler, Armand Mariscal, Jean-Marc Nicole, Özgür Tuna Özmen, Carsten Riggelsen, Abdullah Sandıkkaya, Paula Teves-Costa, Bekir Tüzel, Daniel Vollmer and Ali Zeynel. This work has been supported by the European NERIES project. We thank the editor Jeannot Trampert and the reviewer Michele Cercato for constructive remarks and accurate reviews which helped to greatly improve the manuscript.

REFERENCES

Aki, K., 1957. Space and time spectra of stationary stochastic waves, with special reference to microtremors, *Bull. Earthq. Res. Inst. Tokyo Univ.,* **35,** 415–456.

Albarello, D. & Lunedei, E., 2010. Alternative interpretations of horizontal to vertical spectral ratios of ambient vibrations: new insights from theoretical modeling, *Bull. Earthq. Eng.,* **8,** 519–534.

Albarello, D. & Lunedei, E., 2011. Structure of an ambient vibration wavefield in the frequency range of engineering interest ([0.5, 20] Hz): insights from numerical modeling, *Near Surf. Geophys.,* **9,** 543–559.

Arai, H. & Tokimatsu, K., 2004. S-wave velocity profiling by inversion of microtremor H/V spectrum, *Bull. seism. Soc. Am.,* **94,** 53–63.

Arai, H. & Tokimatsu, K., 2005. S-wave velocity profiling by joint inversion of microtremor dispersion curve and horizontal-to-vertical (H/V) spectrum, *Bull. seism. Soc. Am.,* **95,** 1766–1778.

Asmussen, J.C., 1997. Modal analysis based on the random decrement technique, *Ph.D. thesis,* University of Aalborg, Denmark.

Bard, P.-Y. *et al.*, 2010. From non-invasive site characterization to site amplification: recent advances in the use of ambient vibration measurements, in *Earthquake Engineering in Europe,* Vol. 17: Geotechnical, Geological and Earthquake Engineering, pp. 105–123, eds Garevski, M. & Ansal, A., Springer, Dordrecht, Heidelberg, London, New York.

Bettig, B., Bard, P.-Y., Scherbaum, F., Riepl, J., Cotton, F., Cornou, C. & Hatzfeld, D., 2001. Analysis of dense array noise measurements using the modified spatial auto-correlation method (SPAC): application to the Grenoble area, *Boll. Geof. Teor. Appl.,* **42,** 281–304.

Bonnefoy-Claudet, S., Köhler, A., Cornou, C., Wathelet, M. & Bard, P.-Y., 2008. Effects of Love waves on microtremor H/V ratio, *Bull. seism. Soc. Am.,* **98,** 288–300.

Boore, D.M. & Toksöz, M.N., 1969. Rayleigh wave particle motion and crustal structure, *Bull. seism. Soc. Am.,* **59,** 331–346.

Calderón-Macías, C. & Luke, B., 2007. Improved parameterization to invert Rayleigh-wave data for shallow profiles containing stiff inclusions, *Geophysics,* **72,** U1–U10.

Capon, J., 1969. High-resolution frequency-wavenumber spectrum analysis, *Proc. IEEE,* **57,** 1408–1418.

Cercato, M., 2009. Addressing non-uniqueness in linearized multichannel surface wave inversion, *Geophys. Prospect.,* **57,** 27–47.

Cercato, M., 2011. Global surface wave inversion with model constraints, *Geophys. Prospect.,* **59,** 210–226.

Cercato, M., Cara, F., Cardarelli, E., Di Filippo, G., Di Giulio, G. & Milana, G., 2010. Shear-wave velocity profiling at sites with high stiffness contrasts: a comparison between invasive and non-invasive methods, *Near Surf. Geophys.,* **8,** 75–94.

Cornou, C., Ohrnberger, M., Boore, D.M., Kudo, K. & Bard, P.-Y., 2009. Derivation of structural models from ambient vibration array recordings: results from an international blind test, in *Proc. 3rd Int. Symp. on the Effects of Surface Geology on Seismic Motion,* LCPC Editions, Grenoble, 30 August–01 September, 2006, Vol. 2, pp. 1127–1217.

Di Giulio, G. *et al.*, 2012. Exploring the model space and ranking a best class of models in surface-wave dispersion inversion: application at European strong motion sites, *Geophysics,* **77,** B147–B166.

Dunand, F., 2005. Pertinence du bruit de fond sismique pour la caractérisation dynamique et l'aide au diagnostic sismique des structures de génie civil, *PhD thesis,* Université Joseph Fourier Grenoble.

Dunkin, J.W., 1965. Computation of modal solutions in layered, elastic media at high frequencies, *Bull. seism. Soc. Am.,* **55,** 335–358.

Endrun, B., 2011. Love wave contribution to the ambient vibration H/V amplitude peak observed with array measurements, *J. Seismol.,* **15,** 443–472.

Endrun, B. & Renalier, F., 2008. Report on in-situ measurements at the 20 selected sites, NERIES deliverable JRA4 D2. Available at: http://www.neries-eu.org (last accessed 2012 October 25).

Fäh, D., Kind, F. & Giardini, D., 2001. A theoretical investigation of average H/V ratios, *Geophys. J. Int.,* **145,** 535–549.

Fäh, D., Kind, F. & Giardini, D., 2003. Inversion of local S-wave velocity structures from average H/V ratios, and their use for the estimation of site-effects, *J. Seismol.,* **7,** 449–467.

Ferreira, A.M.G. & Woodhouse, J.H., 2007. Observations of long period Rayleigh wave ellipticity, *Geophys. J. Int.,* **169,** 161–169.

Haskell, N.A., 1953. The dispersion of surface waves on multilayered media, *Bull. seism. Soc. Am.,* **43,** 17–34.

Hobiger, M., 2011. Polarization of surface waves: characterization, inversion and application to seismic hazard assessment, *PhD thesis,* Université de Grenoble, France.

Hobiger, M., Bard, P.-Y., Cornou, C. & Le Bihan, N., 2009. Single station determination of Rayleigh wave ellipticity by using the random decrement technique (RayDec), *Geophys. Res. Lett.,* **36,** L14303, doi:10.1029/2009GL038863.

Köhler, A., Ohrnberger, M. & Scherbaum, F., 2006. The relative fraction of Rayleigh and Love waves in ambient vibration wavefields at different European sites, in *Proceedings of the 3rd Int. Symp. on the Effects of Surface Geology on Seismic Motion,* Grenoble, 30 August–01 September, Vol. 1, pp. 351–360.

Konno, K. & Ohmachi, T., 1998. Ground-motion characteristics estimated from spectral ratio between horizontal and vertical components of microtremor, *Bull. seism. Soc. Am.,* **88,** 228–241.

Liang, Q., Chen, C., Zeng, C., Luo, Y. & Xu, Y., 2008. Inversion stability analysis of multimode Rayleigh-wave dispersion curves using low-velocity layer models, *Near Surf. Geophys.,* **6,** 157–165.

Malischewsky, P.G. & Scherbaum, F., 2004. Love's formula and H/V-ratio (ellipticity) of Rayleigh waves, *Wave Motion,* **40,** 57–67.

Maranò, S., Reller, C., Loeliger, H.-A. & Fäh, D., 2012. Seismic waves estimation and wavefield decomposition: application to ambient vibrations, *Geophys. J. Int.,* **191,** 175–188.

Michel, C., Guéguen, P. & Bard, P.-Y., 2008. Dynamic parameters of structures extracted from ambient vibration measurements: an aid for the seismic vulnerability assessment of existing buildings in moderate seismic hazard regions, *Soil Dyn. Earthq. Eng.,* **28,** 593–604.

Morikawa, H., Sawada, S. & Akamatsu, J., 2004. A method to estimate phase velocities of Rayleigh waves using microseisms simultaneously observed at two sites, *Bull. seism. Soc. Am.,* **94,** 961–976.

Nakamura, Y., 1989. A method for dynamic characteristics estimation of subsurface using microtremor on the ground surface, Quarterly reports of the Railway Technical Research Institute Tokyo, Japan, Vol. 30, pp. 25–33.

Nogoshi, M. & Igarashi, T., 1971. On the amplitude characteristics of microtremor (part 2), *J. Seism. Soc. Japan,* **24,** 26–40 (in Japanese with English abstract).

Okada, H., 2006. Theory of efficient array observations of microtremors with special reference to the SPAC method, *Explor. Geophys.,* **37,** 73–85.

O'Neill, A. & Matsuoka, T., 2005. Dominant higher surface-wave modes and possible inversion pitfalls, *J. Environ. Eng. Geophys.,* **10,** 185–201.

Park, C.B., Miller, R.D. & Xia, J., 1999. Multichannel analysis of surface waves, *Geophysics,* **64,** 800–808.

Parolai, S., Picozzi, M., Richwalski, S.M. & Milkereit, C., 2005. Joint inversion of phase velocity dispersion and H/V ratio curves from seismic noise recordings using a genetic algorithm, considering higher modes, *Geophys. Res. Lett.,* **32,** L01303, doi:10.1029/2004GL021115.

Picozzi, M., Parolai, S. & Richwalski, S.M., 2005. Joint inversion of H/V ratios and dispersion curves from seismic noise: estimating the S-wave velocity of bedrock, *Geophys. Res. Lett.,* **32,** L11308, doi:10.1029/2005GL022878.

Picozzi, M. *et al.*, 2007. Selected sites and available information, NERIES deliverable JRA4 D1. Available at http://www.neries-eu.org (last accessed 2012 October 25).

Poggi, V. & Fäh, D., 2010. Estimating Rayleigh wave particle motion from three-component array analysis of ambient vibrations, *Geophys. J. Int.,* **180,** 251–267.

Poggi, V., Fäh, D., Burjanek, J. & Giardini, D., 2012. The use of Rayleigh wave ellipticity for site-specific hazard assessment and microzonation: application to the city of Lucerne, Switzerland, *Geophys. J. Int.,* **188,** 1154–1172.

Raptakis, D., Theodulidis, N. & Pitilakis, K., 1998. Data analysis of the Euroseistest strong motion array in Volvi (Greece): standard and horizontal-to-vertical spectral ratio techniques, *Earthq. Spectra,* **14,** 203–224.

Renalier, F. & Endrun, B., 2009. Comparative analysis of classical measurements and newly developed methods, NERIES deliverable JRA4 D6. Available at http://www.neries-eu.org (last accessed 2012 October 25).

Sambridge, M., 1999a. Geophysical inversion with a neighbourhood algorithm - I. Searching a parameter space, *Geophys. J. Int.,* **138,** 479–494.

Sambridge, M., 1999b. Geophysical inversion with a neighbourhood algorithm - II. Appraising the ensemble, *Geophys. J. Int.,* **138,** 727–746.

Sánchez-Sesma, F.J. *et al.*, 2011. A theory for microtremor H/V spectral ratio: application for a layered medium, *Geophys. J. Int.,* **186,** 221–225.

Satoh, T., Kawase, H., Iwata, T., Higashi, S., Sato, T., Irikura, K. & Huang, H.-C., 2001. S-wave velocity structure of the Taichung Basin, Taiwan, estimated from array and single-station records of microtremors, *Bull. seism. Soc. Am.,* **91,** 1267–1282.

Scherbaum, F., Hinzen, F.K. & Ohrnberger, M., 2003. Determination of shallow shear wave velocity profiles in the Cologne, Germany area using ambient vibrations, *Geophys. J. Int.,* **152,** 597–612.

Socco, L.V. & Strobbia, C., 2004. Surface-wave method for near-surface characterization: a tutorial, *Near Surf. Geophys.,* **2,** 165–185.

Tanimoto, T. & Alvizuri, C., 2006. Inversion of the HZ ratio of microseisms for S-wave velocity in the crust, *Geophys. J. Int.,* **165,** 323–335.

Thomson, W.T., 1950. Transmission of elastic waves through a stratified solid medium, *J. appl. Phys.,* **21,** 89–93.

Tuan, T.T., Scherbaum, F. & Malischewsky, P.G., 2011. On the relationship of peaks and troughs of the ellipticity (H/V) of Rayleigh waves and the transmission response of single layer over half-space models, *Geophys. J. Int.,* **184,** 793–800.

Uebayashi, H., Kawabe, H. & Kamae, K., 2012. Reproduction of microseism H/V spectral features using a three-dimensional complex topographical model of the sediment-bedrock interface in the Osaka sedimentary basin, *Geophys. J. Int.,* **189,** 1060–1074.

Wathelet, M., 2005. Array recordings of ambient vibrations: surface-wave inversion, *PhD thesis,* Université de Liège, Belgium.

Wathelet, M., 2008. An improved neighborhood algorithm: parameter conditions and dynamic scaling, *Geophys. Res. Lett.,* **35,** L09301, doi:10.1029/2008GL033256.

Wathelet, M., Jongmans, D. & Ohrnberger, M., 2004. Surface wave inversion using a direct search algorithm and its application to ambient vibration measurements, *Near Surf. Geophys.,* **2,** 211–221.

Wathelet, M., Jongmans, D., Ohrnberger, M. & Bonnefoy-Claudet, S., 2008. Array performances for ambient vibrations on a shallow structure and consequences over V_S inversion, *J. Seismol.,* **12,** 1–19.

Xia, J., Miller, R.D., Park, C.B. & Tian, G., 2003. Inversion of high frequency surface waves with fundamental and higher modes, *J. appl. Geophys.,* **52,** 45–57.

Yamanaka, H., Takemura, M., Ishida, H. & Niwa, M., 1994. Characteristics of long-period microtremors and their applicability in exploration of deep sedimentary layers, *Bull. seism. Soc. Am.,* **84,** 1831–1841.

Yano, T., Tanimoto, T. & Rivera, L., 2009. The ZH ratio method for long-period seismic data: inversion for S-wave velocity structure, *Geophys. J. Int.,* **179,** 413–424.

SUPPORTING INFORMATION

Additional Supporting Information may be found in the online version of this article:

Detailed inversion results for the remaining 12 sites
(http://gji.oxfordjournals.org/lookup/suppl/doi:10.1093/gji/ggs005/-/DC1)

Please note: Oxford University Press is not responsible for the content or functionality of any supporting materials supplied by the authors. Any queries (other than missing material) should be directed to the corresponding author for the article.